Helsinki University of Technology

Department of Materials Science and Engineering

Fiseha Tesfaye Firdu

Kinetics of Copper Reduction from Molten Slags

A thesis presented for examination for the degree for Master of Science in Engineering in Espoo, August 2009.

Supervisor: _____

Professor Michael Gasik

Instructor: _____

M.Sc. (Tech.) Kruskopf Ari

Preface

This thesis was carried out in the Laboratory of Materials Processing and Powder Metallurgy at Helsinki University of Technology from January 2009 to June 2009. It is part of a project that aims to improve slag cleaning process in an electric furnace.

I am deeply grateful to my supervisor, Professor Michael Gasik, for his dedicative supervision and guidance during my work. Ideally everyone should have a supervisor as good as Professor Gasik. I would also like to thank my instructor Kruskopf Ari, M.Sc. (Tech.), for his help and advice during the work and his helpful comments and input into both the planning and actual carrying out of my work.

Special thanks are due to Professor Pekka Taskinen for his comments, discussions and valuable inputs into this work.

I would also like to thank Outotec Research Oy for their financial support. Thanks also to the personnel of the Laboratory of Materials Processing and Powder Metallurgy for all their help and for creating such a pleasant working atmosphere.

Finally, the warmest thanks to my wife Anne and my parents for their trust, encouragement and support during my study.

Espoo, August 2009

Fiseha Tesfaye Firdu

TEKNILLINEN KORKEAKOULU **DIPLOMITYÖN TIIVISTELMÄ**

Tekijä:	Fiseha Tesfaye Firdu
Työn nimi:	Kuparin pelkistämisen kinetiikka sulakuonasta
Päivämäärä:	30.06.2009
Sivumäärä:	84
Osasto:	Materiaalitekniikan laitos
Professuuri:	Materiaalien valmistustekniikka ja jauhemetallurgia
Työn valvoja:	Professori Michael Gasik
Työn ohjaaja:	Kruskopf Ari, DI.
Avainsanat:	Fajaliittinen kuona, kuonanpuhdistus, koostumus, korkealämpötila hiilipelkistys-reaktio, pelkistyminen, Cu_2O, FeO_x.

Työn tarkoituksena oli tutkia kupari(I)oksidin (Cu_2O) hiilipelkistystä kupari - liekkisulatusuunista tulevasta kuonasta.

Liekkisulatus - ja kuonan puhdistusprosessit on kuvailtu johdanto-osassa. Tutkimukset ovat keskittyneet kuonanpuhdistuksen kemiaan kolme-elektrodisessa sähköuunissa, jossa kuonan komponentit jakautuvat jätekuonaksi ja kuparikiveksi panosprosessissa. Erilaisten muuttujien (pintajännitys, tiheys, viskositeetti ja tasapainokoostumus) parametriset arvot ja pelkistymisreaktion termodynamiikka kuonanpuhdistus- prosesissa on myös tutkittu. Korkeassa hapen osapaineessa CaO:n ja MgO:n lisäys suurentaa Cu_2O:n ja Fe_2O_3:n aktiivisuuskertoimia, joten Cu_2O:n konsentraatio ja Fe^{+3}/Fe^{+2} – suhde pienenevät. Lisäksi emäksisten oksidien kohtuulliset lisäykset rikkovat $(SiO_4)^{4-}$ ketjut pienentäen kuonan viskositeettiä.

Cu_2O:n ja Fe_2O_3:n pelkistymiskinetiikka on tutkittu kirjallisuustyönä. Erilaisten muuttujien (lämpötila, alkukonsentraatio ja reaktiotuotteet) vaikutusta Cu_2O:n pelkistymiskinetiikkaan on analysoitu lämpötilavälillä 1200 – 1650^{o}C, joka on havaittu parhaaksi lämpötila- alueeksi kuonanpuhdistusprosessissa.

Sekä termodynamiikan että kinetiikan analyysien tulokset vahvistivat lämpötilan nostamisen nopeuttavan Cu_2O:n ja FeO_x:n pelkistymistä. Pelkistymisnopeuksien aikaisemmin oletettiin olevan ensimmäisen kertaluvun reaktio konsentraation suhteen ja reaktionopeuden rajoittaja oli kemiallinen reaktio kuona-koksi-rajapinnalla. Tässä analyysissä Fe_2O_3 pelkistymisen on todettu olevan ensimmäisen kertaluvun reaktio, mutta kupari(I)oksidin pelkistymisen havaittiin olevan autokatalyyttinen.

HELSINKI UNIVERSITY OF TECHNOLOGY **ABSTRACT OF MASTER'S THESIS**

Author:	Fiseha Tesfaye Firdu
Title of the thesis:	Kinetics of Copper Reduction from Molten Slags
Date:	30.06.2009
Number of pages:	84
Department:	Department of Materials Science and Engineering
Chair:	Materials Processing and Powder Metallurgy
Supervisor:	Professor Michael Gasik
Instructor:	Kruskopf Ari, M.Sc.(Tech.)
Keywords:	Fayalitic slags, slag cleaning, carbothermic reaction, composition, reduction, Cu_2O, FeO_x.

The objective of this thesis was to study the process of reduction of cuprous oxide by carbon from copper flash smelting slags.

The flash smelting and slag cleaning processes are described in the introductory part. The studies are focused on the slag cleaning process in the three - electrode electric furnace (EF), where components of the slag reduce to matte and EF slag in a periodic batch process. Parametric values of different variables (surface energy, density, viscosity, and equilibrium composition) and thermodynamics of reduction reactions of the slag cleaning process were also examined. At higher oxygen potential additions of CaO and MgO were found to increase the activity coefficient of both Cu_2O and Fe_2O_3, thereby reducing the amount of Cu_2O and Fe^{+3}/Fe^{+2} ratio in the slag. Furthermore, reasonable additions of the basic oxides will break the $(SiO_4)^{4-}$ chains and reduce viscosity of the slag.

Kinetics of reduction of Cu_2O and FeO_x were reviewed based on data obtained from different publications. Effects of various variables such as temperature, initial composition and reaction products on the reduction kinetics of Cu_2O were analyzed in the temperature range of 1200 - 1650^{o}C, which was identified to be the most favorable in the slag cleaning process.

Results from both thermodynamic and kinetic analyses confirmed that increase in temperature increase the reduction rates of both Cu_2O and FeO_x. The reduction rates of the oxides were widely accepted to be the 1st order reaction with respect to their concentration and the rates limiting step was chemical reaction at the slag-coke interface. In this analysis the reduction of Fe_2O_3 was confirmed to follow the 1st order reaction, but the reduction of Cu_2O was found to be autocatalytic.

Table of Contents

Nomenclature

T	temperature	[K]
γ	surface/interfacial tension	[N·m^{-1}]
ρ	density	[kg·m^{-3}]
μ	dynamic viscosity	[kg·m^{-1}·s^{-1}], [Pa·s]
$a_{Me/MeO}$	activity of components in the slag	[-]
$\Delta G_{reaction}$	Gibbs free energy change of a reaction	[J·mol^{-1}]
r_o	critical radius	[m]
r	radius	[m]
A_r	reaction surface area	[m^2]
g	gravitational acceleration	[m·s^{-2}]
$[\mathrm{MO_x}]$	concentration of metal oxide	[wt. % MO_x]
$[\mathrm{MO_x}]_o$	initial concentration of metal oxide	[wt. % MO_x]
$[\mathrm{MO_x}]_t$	instantaneous concentration of metal oxide	[wt. % MO_x]
t	time	[s]
$\frac{d[MO_x]}{dt}$	reduction rate of metal oxide	[wt. % MO_x·s^{-1}]
k	apparent rate constant (1st order reaction)	[s^{-1}]
K_o	frequency factor (1st order reaction)	[s^{-1}]

1 Introduction

The latest copper smelting technologies adopt excessive use of oxygen to increase the smelting capacity thereby enabling a highly efficient and environmentally acceptable smelting process. However, improving the grade of matte has some drawbacks such as increased copper loss in slag. It has been shown that when the copper grade of matte exceeds 70% Cu , the oxygen potential in the slag-matte system increases drastically, leading to copper loss to the slag predominantly in the form of cuprous oxide [1].

Owing to the technological advances in copper extraction, the amount of copper loss (in oxide form) to this day's slags increased beyond 1 wt. % up to 2 wt. % in matte smelting [2] and up to 25 wt. % in direct-to- blister smelting. Hence the recent trends of continuous copper smelting invariably lead to significant copper loss in slag, which needs to be recovered by means of reduction and settling in a separate slag cleaning furnace.

Reduction of iron oxides from slags using carbon as a reductant in the form of dissolved carbon in iron or graphite has been studied extensively by a large number of researchers. A number of researches were performed on recovery of metallic values from copper smelting slags. However, little information is available in literature concerning the reduction kinetics of cuprous oxide using coke from fayalitic slags.

From the industrial point of view, knowledge of the reactions at the slag-coke interface is important for optimizing process parameters in a copper recovery processes. Thus, the main purpose of this study is to estimate the reduction rate of Cu_2O by carbon from fayalitic slags which are similar to the industrial copper flash smelting furnace slags.

In summary, effects of additives on the equilibrium composition and physical properties of the slag were reviewed. Carbothermic reaction of the competing metal oxides (Cu_2O and FeO_x) at the slag-coke interface was thermodynamically studied. The critical sizes of reaction products (Cu-drops and CO-bubbles) at detachment from the coke surface and their rise/fall speeds after that were estimated, based on physical properties of the molten slag components at particular conditions. The reduction rate of cuprous oxide by carbon from synthetically prepared slags was literarily studied. The effect of temperature and initial concentrations on the reduction rate, and the controversial reduction mechanisms were reviewed.

1.1 Flash Smelting Technology

Outokumpu's FSF, invented in response to the 1940s electric energy shortage in Finland, and Flash Converting Furnace (FCF) are the leading technologies either in efficiency or environmentally sound method of copper, nickel and lead production with low investment and operating costs. About 50 % of world copper production and 30% of world nickel production comes out of plants which use these technologies.

The main advantages of the Outokumpu FSF processes are the high sulfur recovery, the efficient energy utilization (it needs only 20 to 30% of that required by a conventional furnace) and the flexible process in terms of accepting a varied feed material. Preheated oxygen-enriched air is used to provide heat in such a manner that additional fuel is not required for the reactions to proceed; the reactor shaft is separately illustrated in Figure 1. In the reaction shaft; a suspension of gas, solid concentrate particles and solid flux particles is formed and reactions like the one described below takes place, after spontaneous ignition at 400-600^{o}C:

$2CuFeS_2$ (chalcopyrite) + $5/2O_2$ + SiO_2 (flux) = $Cu_2S{\cdot}FeS$ (matte) + $2FeO{\cdot}SiO_2$ (slag) + $2SO_2$ (g) + heat

When the suspension leaves the reaction shaft, the reacted molten concentrate particles and inert flux particles are separated from the gas stream and hit toward the settler, forming molten slag and matte. In the molten bath, matte and slag will be separated in the settler of the furnace as respective layers due to their difference in density. The matte is sent for further treatment to converter to obtain blister copper. The slag is sent for valuable metals recovery to electric furnace or disposal. Slag cleaning electric furnace integrated in the Outokumpu Flash Smelting Furnace (FSF) plant is schematically illustrated in appendix A and a typical schematic process flow sheet involving the slag cleaning is shown in Figure 2.

In modern smelters dusts are recovered from the smelter gases for recycling. Above 99% of sulfur is recovered from the concentrate for use in sulfuric acid production, eliminating SO_2 emissions to the environment. Gaseous stream containing 10 - 50 % of SO_2 is thus used for production of sulfuric acid [3].

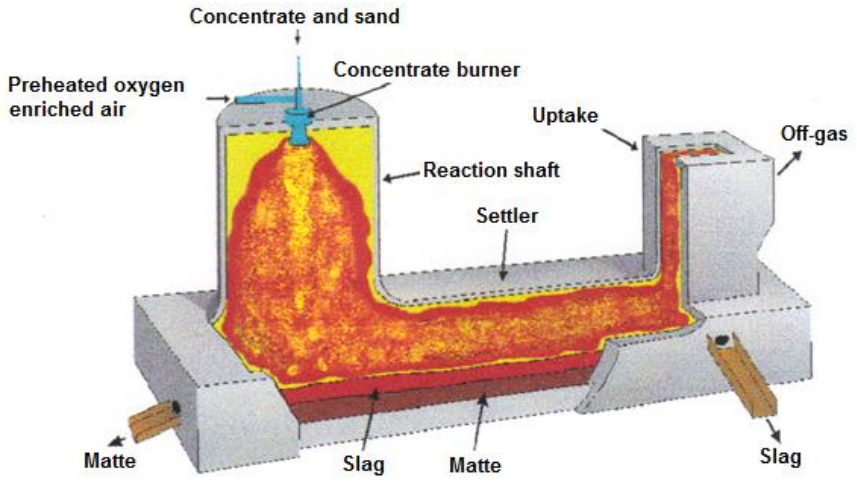

Figure 1. A cut-away diagram of the FSF showing that primary smelting occurs in the reactor shaft [4].

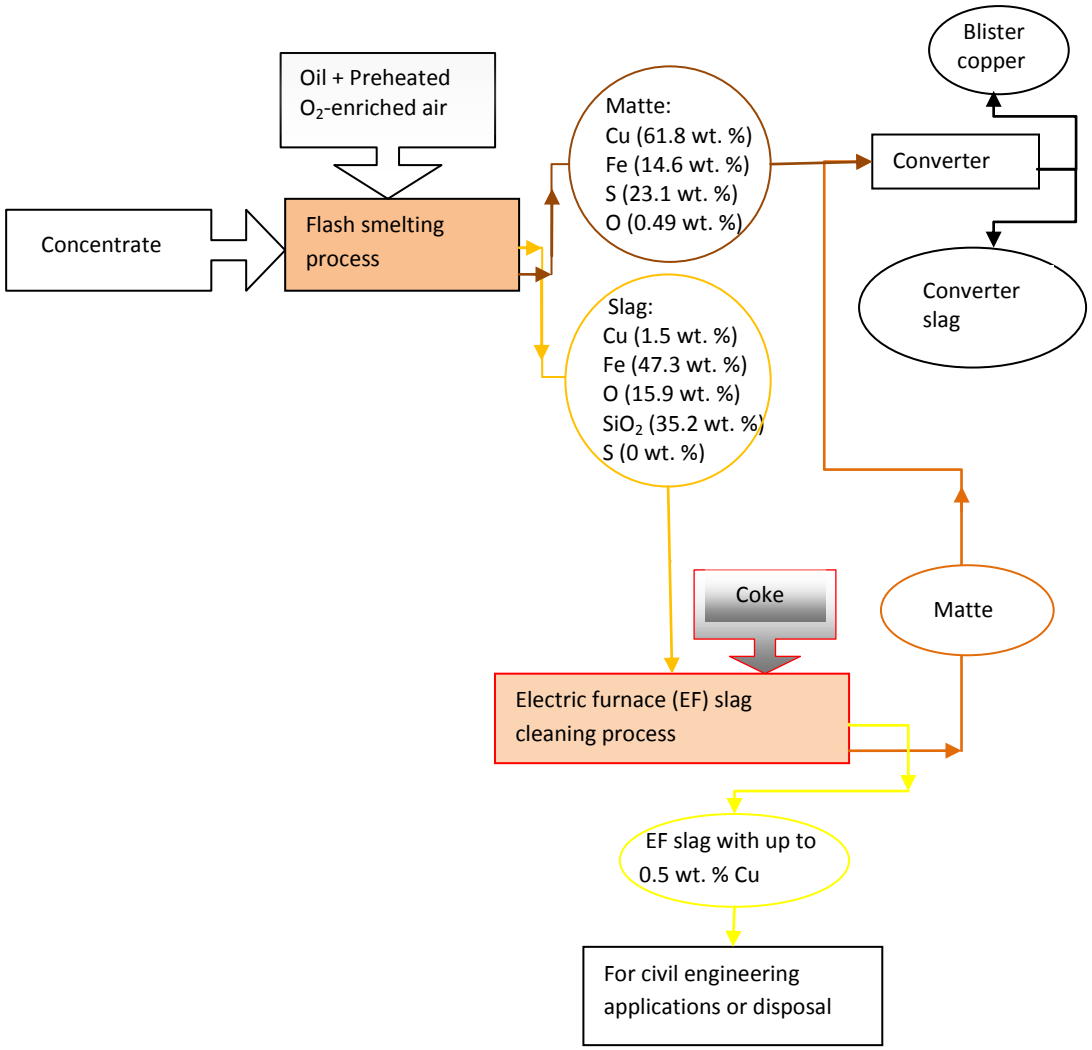

Figure 2. Schematic of process flow sheet of a FSF plant in pyrometallugy of copper.

The lately developed cost effective Outotec's Direct-to-Blister (DB) flash smelting technology, shown in Figure 3, produces slag which contain up to 20-25 % Cu [6]. This makes the slag cleaning process in electric furnace inevitably important. The other end product of the process is blister copper of 98.7% Cu. This is directly sent to the anode furnace to obtain copper of purity 99.3%. DB is suitable and profitable for lower-grade concentrates. The process is currently used on a commercial scale in Zambia, Poland and Australia.

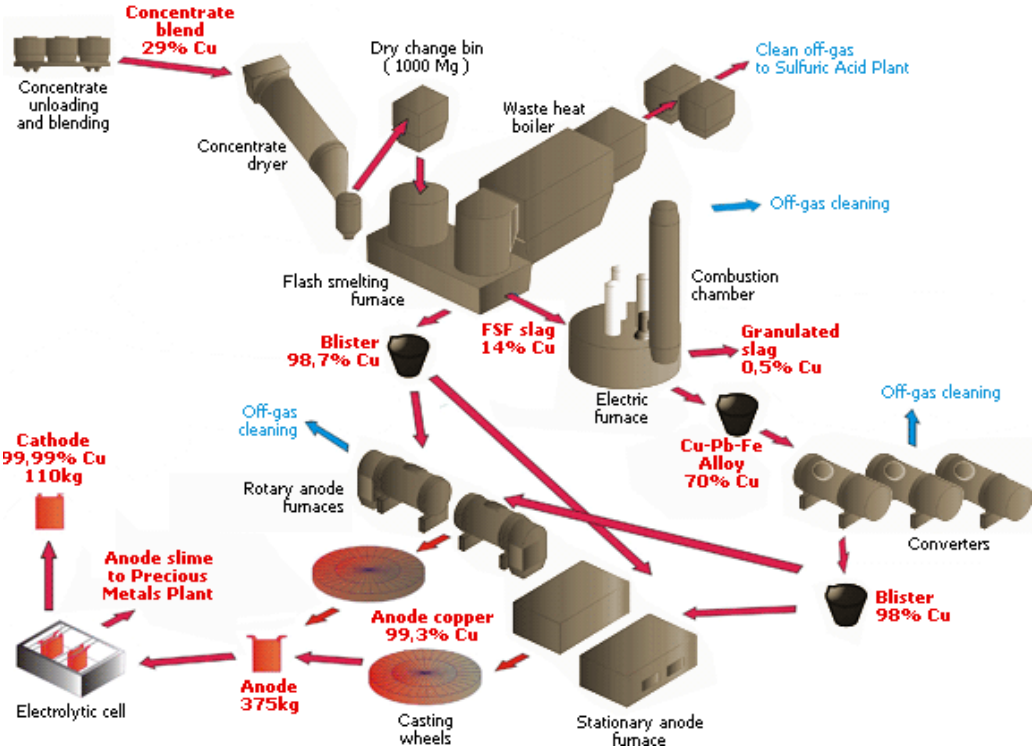

Figure 3. Diagram of the latest Outokumpu's Flash Smelting Process (Direct - to - Blister) showing a single-step process from concentrate to an end product [6].

1.2 Slag Cleaning in an Electric Furnace

Pyrometallurgical slag cleaning processes are usually done in an electric furnace. Slag cleaning in an electric furnace generally consists of heating up the slag to processing temperature, oxide reduction and settling of metal or matte inclusions. The heat necessary for melting is generated by the resistance of the slag to the passage of high current between the Soederberg electrodes immersed in the slag. A three phase AC-electric furnace, shown in Figure 4, is the

most common type of furnace used in the slag cleaning process. Typical parameters of the furnace are listed in Table 1.

Oxides reduction is done by adding coke on the top of the molten slag. The size of inclusions of copper matte in the slag varies in a wide range from micro to millimeters [7].The removal of these inclusions, the rate of magnetite reduction and cuprous oxide co-reduction depend strongly on the slag motion [8], which is mainly induced by convection as a result of lasting temperature gradients in the molten slag. CFD modeling of slag cleaning furnaces introduced valuable information about the mechanisms of heat and mass transfer [9]. Intensive slag motion enhances the mass transfer on to the reaction surfaces and accelerates the coalescence of matte inclusions and nucleated metallic copper droplets [8]. Taking a typical size distribution of matte inclusions, one can see that the phase separation, based on steady settling alone, does not permit lowering the copper content to a desirable level. The wide range of size inclusions and the differences in the settling rates of differently sized droplets cause the droplets to collide and coalescence. This sedimentation rate of either the mechanically entrained inclusions or the newly formed droplets, as a result of the metal oxide reduction, can be estimated from the modified Stokes equation; Hamaker's equation expressed in equation (35) [10]. According to this equation the larger the size of droplet the faster it falls. Thus, bigger droplets "wash out" smaller ones by absorbing them as they fall faster through the slag. The role of slag stirring in the inclusion removal is discussed in detail in reference [7].

After cleaning, the matte is tapped for converting and the slag making oxides such as silica, alumina and magnesium oxides form an inert slag that can be suitable for cement production or for other civil engineering purposes [11].

Table 1. Typical slag cleaning electric furnace parameters [9, 12].

Item	Value
Furnace	
Diameter (Outside)	9.3m
Diameter (Inside)	8.4m
Height	5m
Roof	Suspended
Shell cooling (water)	$80m^3/h$
Transformer	
Type	3-phase
Typical input power	4-6MW
Triangle (taps)	120-220V
Star (taps)	220-390v
Electrodes	
Number	3
Type	Soederberg
Diameter	0.8m
Diameter of Position	2.9m

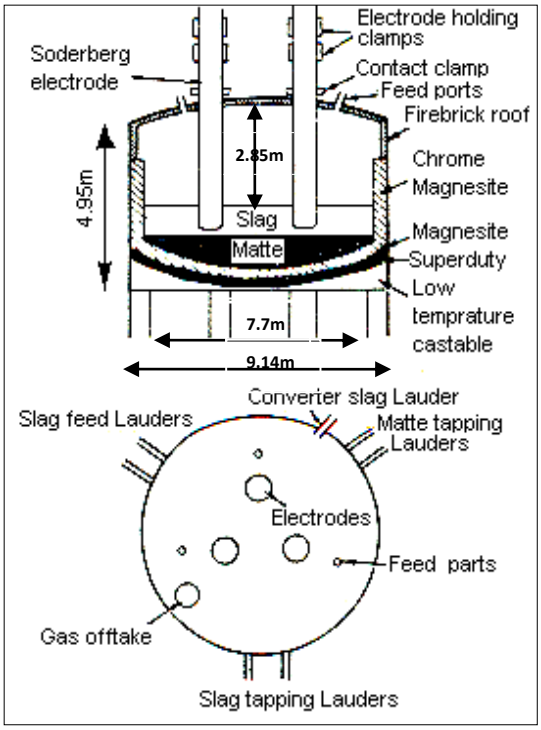

Figure 4. Circular slag cleaning electric furnace [13, 14]. A cut-away schematic diagram of the furnace while operating is shown in Appendix B.

1.3 Physical Properties of Components in the Slag Cleaning Process

Mechanically entrained matte and metal droplets in copper smelting slags originate from various sources such as precipitation of copper from slag due to temperature gradient within the furnace [15] and by vortexing during the slag tapping process [16].

Interfacial tension, density and viscosity are also the factors directly or indirectly responsible for the mechanical loss of the entrained matte and metallic droplets in slag. These physical properties of molten slags largely depend on composition, temperature and partial pressures in the slag. Larger density difference between inclusions and slag, lower slag viscosity (if not too low) and higher interfacial energy would promote inclusions mobility and/or sedimentation.

1.3.1 Surface Energy

Surface energy of molten slags, as the other physical properties, depends on composition. Substances which lower the surface tension of a liquid are termed as surface active substances. Silica is a good example of a surface active substance. It lowers the surface energy of some metal oxides [17]. Nakamura et al. [18] studied the surface energy of Cu_xO-SiO_2 slags in the air at 1573K by maximum bubble pressure method. As a result, it was reported that the surface energy of the slag decreased gradually with the increase in SiO_2 content. In the study the following tendency was also observed: if the surface energy of pure oxide is higher than that of SiO_2, surface energy decreases with an increase of SiO_2 content. On the other hand, if the surface energy of pure oxide is lower than SiO_2, for example, PbO, the surface energy of the binary silicates increases with an increase of SiO_2 content [18]. The non uniform effect of variation of SiO_2 in different molten silicate slags is depicted in Figure 5.

Indifferent to effect of temperature on the other physical properties of slag, surface tension of some slags may increase with temperature [19, 20, 21], as shown in Table 2 below. If the effect of Zn and Pb could be factored out, this reported experimental result would have given formulary relationship of temperature and the physical properties of fayalitic slags.

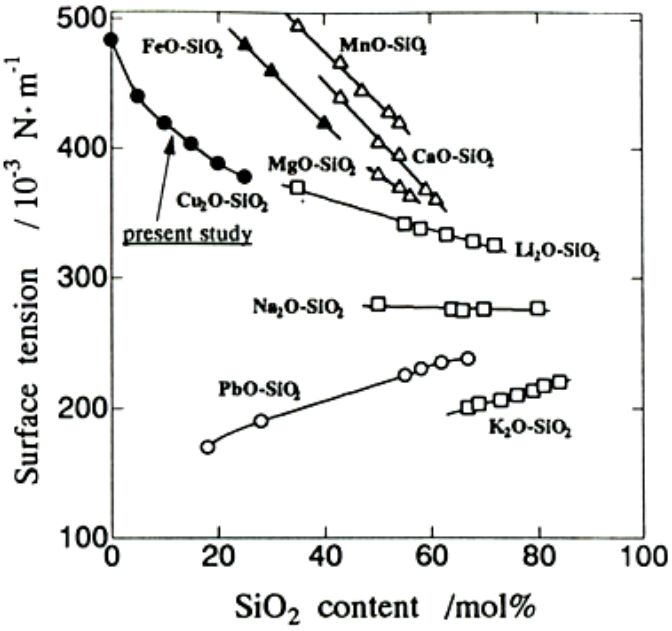

Figure 5. Composition dependence of surface energy in various binary molten silicates at 1573 K [18].

Table 2. The effect of temperature on the three important physical properties of slag and matte [20]. Composition of the slag and matte used in experimental determination of the properties were as defined at the bottom of this table, values in bracket are compositions in wt. %.

Temperature (K)	Slag			Matte		
	μ	γ	ρ	μ	γ	ρ
1573	0.31	0.359	3340	-	0.340	4740
1623	0.26	0.364	3270	-	0.342	4710
1673	0.22	0.370	3210	-	0.345	4680
1723	0.19	0.375	3140	-	0.347	4660
1773	0.16	0.382	3080	-	0.349	4630
1823	0.14	0.387	3020	-	-	-
Slag: Cu(0.31)-FeO(32.4)-S(1.9)-CaO(2.9)-SiO_2(33.8)-Fe_3O_4(3.2)-Al_2O_3(5.1)-Zn(6.3)-Pb(1.2) Matte: Cu(48.9)-FeS(16.48)-S(22.12)-CaO(0.12)-SiO_2(1.3)-Fe_3O_4(-)-Al_2O_3(1.35)-Zn(3.6)-Pb(2.5)						

Knowing the surface energies of each of components in the neighborhood, as distinct phases, enable determination of interfacial tensions between them according to the Girifalco - Good's equation (1) below [15].

$$\gamma_{\text{metal}-\text{slag}} = \gamma_{\text{metal}-\text{gas}} + \gamma_{\text{slag}-\text{gas}} - 2\Phi\sqrt{\gamma_{\text{metal}-\text{gas}} \cdot \gamma_{\text{slag}-\text{gas}}} \quad (1)$$

Utigard et al. [22] studied interfacial tension between iron and slags at different conditions. It has been reported that the interfacial tension between Fe and different slags is a function of the activity of oxygen in the melt (Table 3 and 4). The interaction coefficient (Φ) in the above equation for Fe-slag systems varies according to the composition of melts, for example the value is 0.55 for Fe-Slag III interface and 0.42 for Fe - slag VIII interface [22].

Table 3. Composition of different synthetic slags used by different authors for different experimental studies. Numbers in parenthesis are compositions (wt. %).

Slag No.	Composition
I	Fayalitic copper slag
II	Fayalitic slag (mass ratio: Fe/SiO_2=1.44)
III	SiO_2-CaO-Al_2O_3-FeO
IV	CaO-MgO(12)-SiO_2-FeO(3-20), basicity: CaO/SiO_2=1.2
V	FeO_x-SiO_2 (12-35)
VI	SiO_2(24.2)-CaO(39.8)-Al_2O_3(18.5)-MgO(8.22)-FeO(9.26)
VII	SiO_2(29.6)-CaO(24.4)-FeO(40.76)
VIII	CaF_2-CaO-MgO-FeO
IX	"FeO"(64.1)-SiO_2(29.8)-CaO(2.0)-MgO(0.5)-Al_2O_3(3.6)
X	"FeO"(61.8)-SiO_2(31.7)-CaO(2.0)-MgO(0.4)-Al_2O_3(4.0)

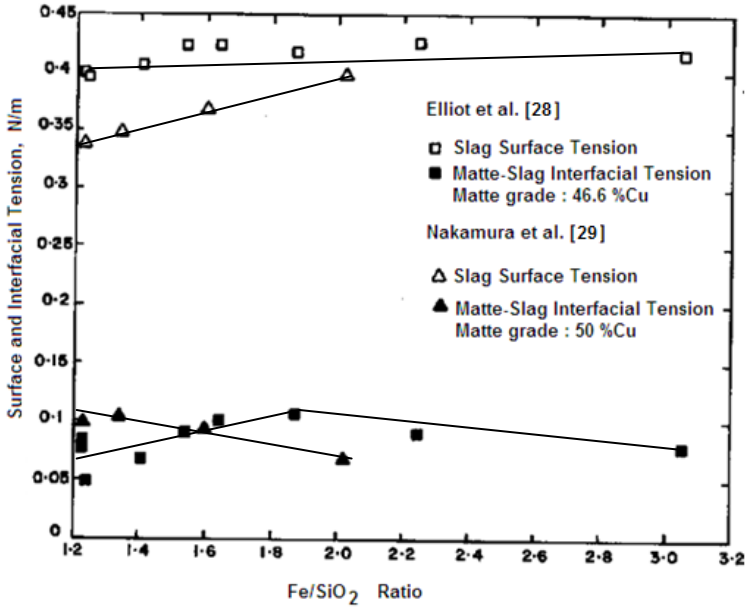

Figure 6. Surface tension of fayalite slag and interfacial tension of copper-matte-slag system as a function of slag composition at 1473K. Interfacial tension data obtained at constant matte grade [15].

In their studies for mechanisms of the droplet entrainment which results from rising gas bubbles, Toguri et al. [15] reported that spreading of copper on bubbles is an impossible event at oxygen partial pressures between 10^{-12}- 10^{-8} atm. The surface tension of the slag used in the study is shown in Figure 6 above.

Table 4. Interfacial energy of some of the interfaces existing in the high temperature copper FSF slag cleaning processes (slag types are listed in Table 3).

Interface	Interfacial energy (J/m^2)	T(K)	Ref.
Matte (inclusion) - slag I	0.15 (70 wt. % Cu in the drop)	1473	[15,23]
	0.1 (60 wt. % Cu in the drop)	1473	[15,23]
Cu - Slag II	0.741	1473	[15]
Cu – matte	0.28	1473	[15]
Cu – gas	1.25	1473	[22]
	1.224	1873	[22]
Fe - gas	1.8-1.9	1473-1573	[22]
(gamma) Fe - gas	1.95	1573	[24]
FeO – gas	0.57	1873	[22]
CuO – gas	0.134	1473	[22]
Slag II - gas	0.25 (Po_2= 10^{-11}atm)	1473	[25]
	0.35 – 0.42	1473	[15]
Slag IV – gas	0.380	1713	[26]
Slag VII – gas	0.335	>1483	[28]
Slag V – gas	0.415 (35 wt. % SiO_2)	>1400	[24]
	0.48 (15 wt. % SiO_2)		[24]
Fe - slag III	1.34	-	[22]
(Fe-C) - slag IV	1.2	1713	[26]
Fe - slag V	1.2	1573	[24]
Solid graphite - gas	0.931	1873	[27]
Coke - slag	0.945	-	[28]
Graphite - slag VI	0.906 using equation (13)	1873	[27]
Graphite - slag VI	0.817 using equation (14)	1873	[27]

1.3.2 Density

Densities of multicomponent oxide melts have been studied by many researchers. It was found to be linearly varying with the temperature, irrespective of composition variations [13, 31].

For instance, in a pure fayalite slag of composition 33 wt. % SiO_2, density of the slag is 3.66 g/cc at 1270^{o}C and 3.58 g/cc at 1509^{o}C [13] .

Iron silicate melts density decrease with the increase of silicon dioxide and basic oxide components such as CaO of the slag as depicted in Figure 7. In the FeO-Fe_2O_3-SiO_2 system an increase in Fe_2O_3 decreases density of the slag at constant Fe/SiO_2 ratio. However, SiO_2 alteration makes the largest variation [13].

Temperature rise reduces the density of matte melts (Cu_2S·FeS) to some extent. An increase in the amount of copper in the matte increases the density of the matte [13]. Thus, density difference between the bulk slag and the matte also increases. The more the amount of copper in matte droplets the easier is the settling of the drops. The densities of some components used in this study are listed in Table 5.

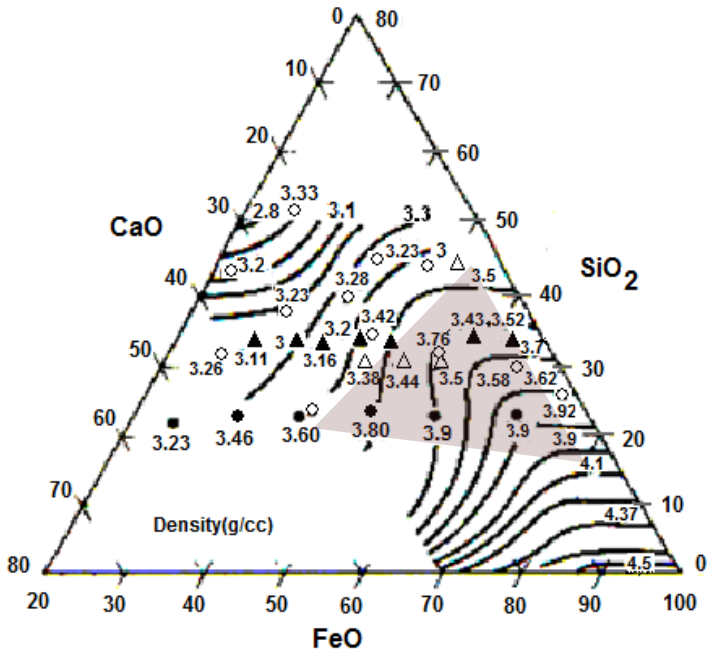

Figure 7. Density of CaO-FeO-SiO_2 melts measured by different investigators. Solid lines represent a temperature range of 1250-1410^{o}C and the rest of marks represent a temperature of about 1410^{o}C [13]. Shaded region indicates slag compositions similar to the copper FSF slags.

Table 5. High temperature density of some important components in slag cleaning process [16, 32, 33].

Material	Density(g/cm^3)	Temperature(K)
Coke	0.95 0.77 (bulk)	-
Slag(l)	2.8 – 3.6	1773 -1473
Copper(l)	7.6	>1358
Matte(l)	4.9	1553
Fe	7.124	1823
Fe-C (3.91wt. %)	7.005	1523

1.3.3 Viscosity

Viscosity, a non-equilibrium property, is a measure of the resistance of a fluid towards motion. It can be related to the tendency of a fluid to dissipate energy (produce entropy) due to internal fluid friction or it can be considered to be momentum conductivity analogous to thermal conductivity in conductive heat transfer and the diffusion coefficient in diffusive mass transfer [19]. Unlike the electrical conductance of silicate melts, where the charge is transferred above all by cations, the transport of momentum in viscous flow is provided mostly by anions [19]. The concept of viscosity can be visualized as in Figure 8.

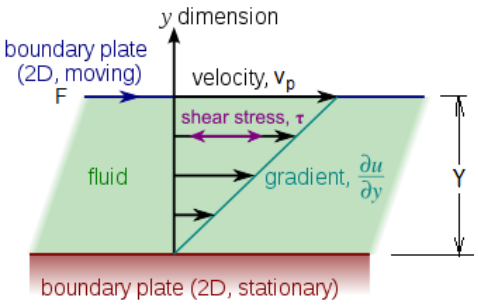

Figure 8. Schematic illustration of viscosity. F: force driving the upper plane and Y: distance between the lower and upper plates.

Figure 8 illustrates a fluid entrained between two parallel plates of area A_p; where the lower plate is fixed while the upper plate is moved at a constant velocity, v_p. After reaching steady

state, the velocity distribution of the fluid will be linear (assuming laminar flow) and the viscosity may be expressed as:

$$\frac{F}{A_p} = \mu \cdot \frac{v_p}{Y}$$

From the above equation the unit of viscosity can be written as Kg/(m.s), for simplicity Pa.s (Pascal-second), which is equal to 10 P(poise), will be used in this study.

Viscosity of molten slags, which largely affect the sedimentation of inclusions in the slag cleaning processes, is sensitive to temperature and composition change. Results reported by different authors and measuring techniques deviate from each other. However, there is a common agreement concerning its variation trend with composition and temperature. For a common Newtonian fluid it decreases rapidly with temperature and always increases with pressure [10]. This is clearly manifested by experimental results in Figure 9, Table 2 and equation (2). Loos et al. [34] derived a relation in equation (2) as a result of two different techniques' average value. Norddeustsche Affinerie electric furnace slag ((0.7-1) wt. % Cu- (31-34) wt. % SiO_2 - (39-41) wt. % Fe - (1.5-3) wt. % Fe_3O_4 - (2-3.5) wt. % CaO - (4-6) wt. % Al_2O_3), in the temperature range 1125 – 1350^{o}C, was used for experimental formulation of the viscosity - temperature relationship below.

$$\mu = 2.817 \cdot 10^{5} \cdot e^{-5.36 \cdot 10^{-3} \cdot T} \qquad (2)$$

Variation of viscosity with the composition at a given temperature is shown in Table 6. In slag reduction processes viscosity of the slag is expected to vary. With the reduction of Fe^{+3} to Fe^{+2} viscosity of fayalitic slags decreases [14, 35, 36]. Studying the variation of viscosity of iron silicate slags, Saarinen et al. [14] reported that at constant temperature viscosity rises along with the SiO_2 amount in the slag. This is because SiO_2 forms $(SiO_4)^{4-}$ chains which produce long "molecules" [35]. FeO tends to reduce viscosity of the slag [14]. The influence of Fe^{+3}/Fe^{+2} ratio and SiO_2 on viscosity can be reduced by the addition of CaO. In the later case CaO splits SiO_2 network and thereby lowers viscosity [2, 14, 35]. However, the amount of CaO in slag may increase the viscosity of silicate slags in the temperature range 1423-1623 K. There exists a minimum in the viscosity - composition isotherms below 1623 K which gets towards the lower CaO content as the temperature falls [2]. The effect of temperature at constant initial composition of the slag can be seen in Table 2.

Table 6. Viscosity of SiO_2-Al_2O_3-CaO-FeO melts [17, 19].

	Composition (wt. %)					Viscosity $(Pa.s)$		
SiO_2	Al_2O_3	CaO	MgO	FeO	Fe_2O_3	1200 °C	1250 °C	1300°C
30	7.7	4.3	-	52.4	5.7	0.87	0.53	0.23
26.2	8.0	4.6	-	53.5	7.7	0.13	0.12	0.10
26.5	8.8	4.3	-	55.0	5.4	0.19	0.13	0.11
25	9.0	4.4	-	57.7	3.9	0.52	0.37	0.23
37.4	8.9	4.9	-	43.6	5.3	0.38	0.27	0.23
27.5	-	17.1	9.68	44.2	1.52	0.575	-	0.36
30.82	-	11.83	-	56.56	0.8	0.45	-	0.4
30.11	-	12.24	0.24	51.36	6.1	-	-	0.44
31.13	0.32	12.3	8.9	33.3	14.1	-	-	0.7

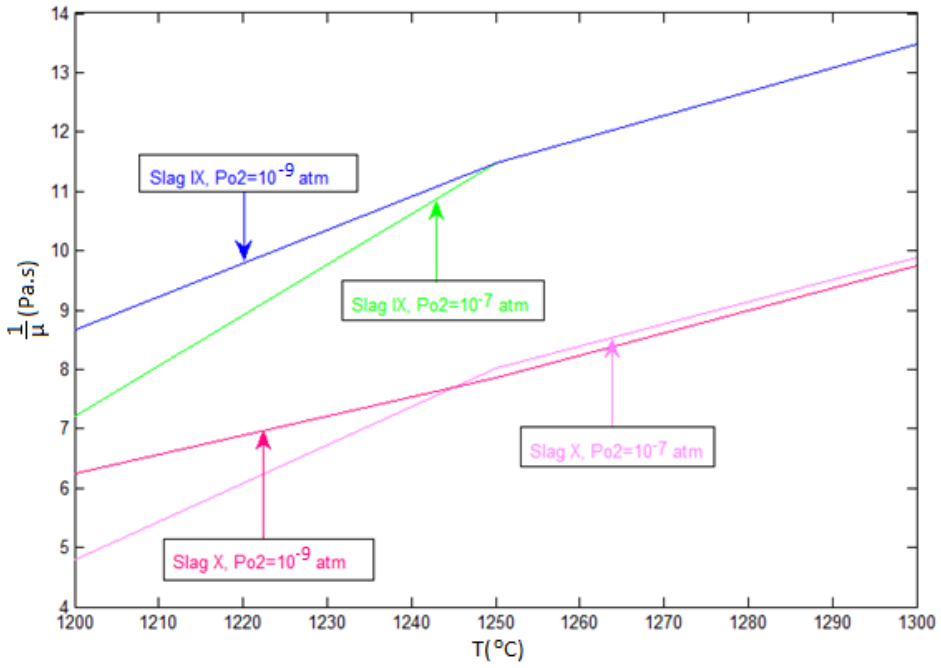

Figure 9. Experimentally determined viscosities of copper slags of mass ratios Fe/SiO_2=1.67 and Fe/SiO_2=1.51, at fixed partial pressures of oxygen. Redrawn from [37], compositions of the slags used for the experimental study are listed in Table 3.

2 Equilibrium Composition and Thermodynamics of Direct Reduction of FSF Slags

Equilibrium composition in molten slags varies with the concentration of influential components in the slag and temperature. For example, the amount of metallic oxides; such as, CaO and MgO, greatly affect the amount of dissolved copper or the activity of Cu_2O and the ferric to ferrous ratio in the slag. In the upper part of the molten slag in an electric furnace the partial pressure of sulfur is low. Thus, to avoid complexity the equilibrium composition of the slag in this study is assumed to be sulfur free.

In spite of the extent of concentration of the components in molten slag, carbon reduction of the metallic oxides is selective. For instance, irrespective of its amount in slag, the reduction of Cu_2O is thermodynamically favored over FeO or ferrous oxide reduction; also ferric oxide reduction to ferrous oxide takes place rapidly. Above the melting point of the slag the Gibbs free energy change of the reduction reactions increase with temperature at the same time obeying the selectivity of the carbothermic reaction, i.e. the Gibbs free energy change of each carbothermic reaction changes with temperature in a similar fashion. The upper limit for the temperature is discussed in section 2.3.2.

2.1 Copper Flash Smelting Slags

Copper flash smelting process produces typically fayalitic slags. The slags contain metals in the form of oxides, sulfides, silicates and ferrites [38]. Appearance of metastable copper-iron-sulfide phase is explained by matte inclusions in the slag. Metallic copper has also been observed by microscopic analysis of these slags after cooling [38]. A typical composition of the copper FSF slag is listed in Table 7.

The copper content of the slag is due to chemical and mechanical reasons. The chemical losses are dictated by the thermodynamic equilibrium of system, which in the case of rich matte (> 60 % Cu) smelting process depends on the oxidation level of the system [16]. A higher oxygen potential results in a higher copper concentration in matte and as a result an increased amount of oxidized copper is departing to the ferrous silicate slag [16]. In addition to the chemical and mechanical losses, matte may be entrained in the slag during tapping by a mechanism called vortexing. The pressure difference between the slag-matte layer and the level of matte (did it rise up to the slag tapping hole?) dictates for this type of copper loss to

the FSF slags [16]. Thus, considering the recent trend of flash smelting techniques the copper content of the slag is mainly in oxide form, and mechanically entrained metal/matte.

Table 7. Chemical composition of the slag considered in this study [5].

Component	Content (wt %)
Cu	1.4-2.8
SiO_2	28
Fe (total)	40
Fe^{+3}	11
Fe_3O_4/FeO	0.73
Al_2O_3	3
CaO	3
MgO	2
S	0.5

2.1.1 Fe-O-SiO_2 system

The main constituents of smelting slags are silica and iron oxides, and consequently the basic silicate constituent is fayalite ($2FeO{\cdot}SiO_2$). The amount of other oxides, charged with concentrate or silica sand as impurities or dissolved from furnace linings, vary within wide limits from smelter to smelter, but rarely exceed 25 wt. % in high grade matte smelting processes [39].

Pyrometallurgy of copper slag systems can be explained by the Fe-O-SiO_2 equilibrium system [13]. Variations of the slag types within the Fe-O-SiO_2 system at different $SiO_2/(SiO_2 + Fe)$ mass ratios and partial pressure of oxygen is depicted in Figure 10 below. According to this phase diagram, the liquid slags maximum oxygen partial pressure is 10^{-7} bar at the Fe_3O_4-SiO_2 dual saturation, and the lowest oxygen partial pressure 10^{-12} bar appears at the Fe-SiO_2 dual saturation.

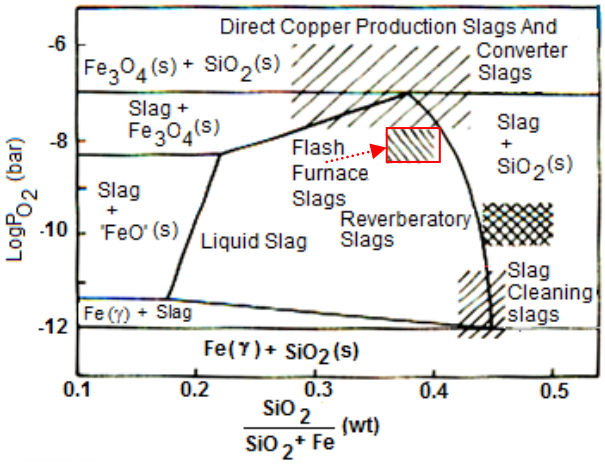

Figure 10. Fe-O-SiO_2 phase diagram at 1523 K showing composition and oxygen pressure of some copper making slags [13]. The arrow indicates the region of FSF slags.

However, the common way of representing iron silicate systems is done through the ternary FeO-Fe_2O_3-SiO_2 equilibrium system, as shown in the FactSage model diagram of Figure 11. This is due to the fact that under normal copper making process conditions the iron activity is very low and ferric oxide activity is relatively high [39].

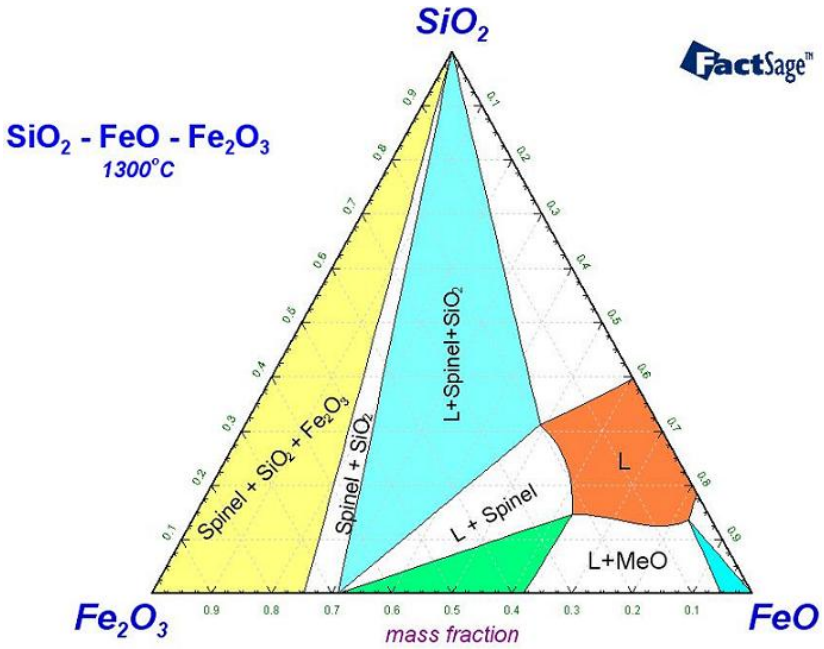

Figure 11. Isothermal phase diagram of FeO-Fe_2O_3-SiO_2 system at 1573K. Calculated using the database 5.4.1 FToxide of FactSage.

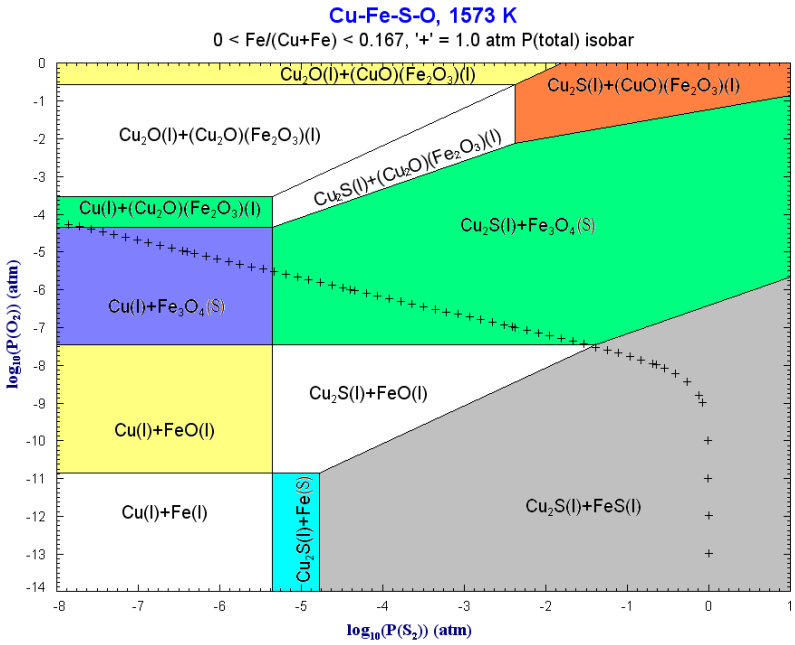

Figure 12. Cu-Fe-S-O system at an isothermal condition of 1573K.

'+' markings in Figure 12 indicate isobaric conditions of total pressure of 1 atm. Higher partial pressure of oxygen and lower partial pressure of sulfur means the system is composed of components of metals and metal oxides. As Figure 12 shows, for $Ps_2<10^{-6}$ atm no sulfide exists in the Cu-Fe-S-O system, no matter how the partial pressure of oxygen changes. At the same condition of Ps_2; for $10^{-5} < Po_2 <10^{-4}$ atm metallic copper, cuprous oxide and ferric oxide exist in the system, and for $10^{-11}<Po_2< 10^{-8}$ atm only metallic copper and ferrous oxide appear. Thus, at $Ps_2<10^{-6}$ atm the Cu-Fe-S-O system can be assumed to be Cu-Fe-O system, which is the case at the slag-coke interface where both partial pressures are at their minimum.

The effect of basic oxides additions (Table 8) on the Fe-O-SiO_2 system is tremendous. This effect is explained in section 1.1 as the change of physical properties of the fayalitic slags. In isothermal systems, illustrated in Figures 10 and 11, addition of CaO (up to 20 wt %) increases the dissolution of SiO_2 in the slag [13]. The variation of activity of metal oxides with temperature in slag is shown in Figure 13 below.

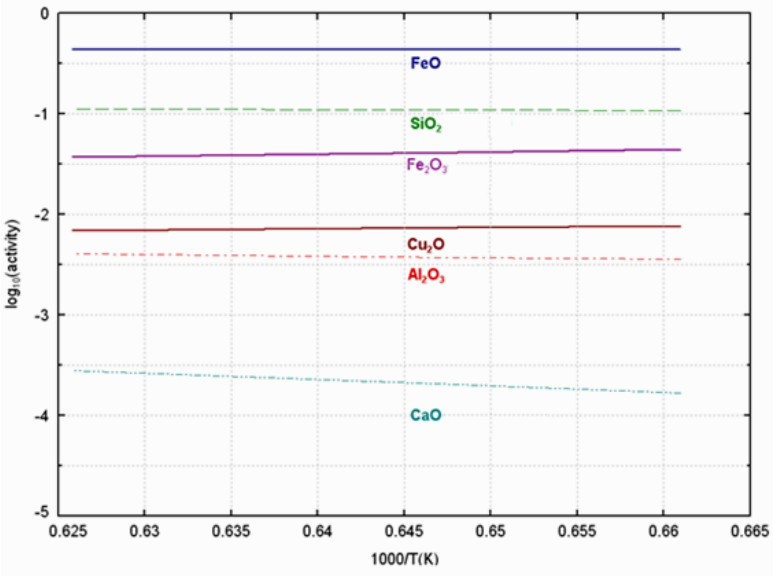

Figure 13. Plot of logarithm of activity of oxides in slag XI (Table 3) vs. inverse of temperature of the slag, at standard states.

Table 8. Compositions of synthetic slags used by different investigators in studying additive effects on fayalitic slags.

	Additives to FeO_x-SiO_2 system		
Code	CaO	Al_2O_3	MgO
1	-	-	-
2	3.5 - 4.5	-	-
3	-	3.5 - 4.5	-
4	-	-	3.5 - 4.5
5	11.9	-	-
6	-	8.2	-
7	3.5-4.5	3.5 - 4.5	-
8	3.5-4.5	3.5 - 4.5	2
9	8	-	-
10	2	3.5 - 4.5	0 – 1

In investigating the concentrate chemistry change, Hector et al. [40] studied the effect of CaO and MgO addition in synthetic slags (Table 8) on the tridymite (SiO_2) and spinel (Fe_3O_4)

liquidus, at a fixed concentration of Al_2O_3 (3.3 wt. %) and partial pressure of oxygen (10^{-8} atm). The temperature range of the study was between 1250-1350^{o}C and the amount of the additives varied from 0 – 6 wt. % CaO and 2.2 - 9 wt. % MgO. As a result it was reported that both additives decreased the tridymite liquidus and increased the spinel liquidus (up to 30^{o}C) [40]. As a result, it has been concluded that "moderate" increase of SiO_2 and MgO in the FSF slags should not be too problematic. The spinel liquidus at different Fe/SiO_2 ratios using slag 10 (Table 8) is estimated to vary with the amount of additives as follows [41]:

$$\mathrm{T(^{\circ}C)_{liquidus}} = 1293.51 - \left(\frac{187.177}{\left(\frac{\mathrm{Fe}}{\mathrm{SiO_2}}\right)}\right) + 5.73 \cdot (\mathrm{wt.\,\%\ CaO}) + 3.67 \cdot (\mathrm{wt.\,\%\ MgO}) + 5.52 \cdot (\mathrm{wt.\,\%\ Al_2O_3})$$

According to the above equation, the liquidus temperature at $Po_2 \approx 10^{-9}$ for a composition range given in Table 6 is about 1203^{o}C.

The effect of Al_2O_3's concentration variation on the liquidus temperature of fayalite slags was experimentally studied by Zhao et al. [42]. In the study, where the amount of Al_2O_3 was varied from 0 - 6 wt. %, the following conclusion was drawn: the liquidus temperature of the fayalitic slags (Al_2O_3-"FeO"-CaO-SiO_2 system) decreased by approximately 3 K for each 1 wt. % Al_2O_3 addition.

2.1.2 Ferric to Ferrous Ion Ratio in the Slag

The Fe^{+3}/Fe^{+2} ratio variation due to the addition of CaO, Al_2O_3 and MgO, or mixture of both was studied by Kim et al. [43]. The extent of additives used in the study is listed in Table 8. It was observed that the ferric to ferrous ratio in the slag decreased with the amount of additives, though the effect become negligible with decreasing oxygen potential, as depicted in Figure 14 below.

The ferric to ferrous ratio in a silica saturated iron silicate slag decreases with an increase of fraction of silica in slag. Kim et al. [43] varied the SiO_2 content in the slag (between 40- 48 wt. %) with the amount of additives. As a result it was reported that the increased amount of silica in the slag enhanced the effect of slag additive to reduce the ferric to ferrous ion ratio in the slag.

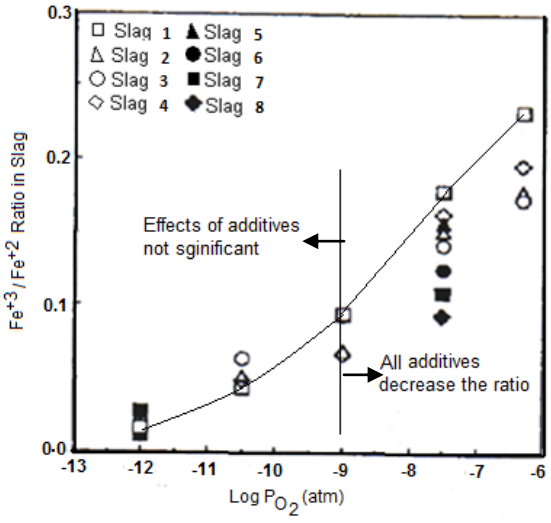

Figure 14. Effect of slag additives on the ratio of the ferric to ferrous ratio in silica-saturated iron silicate slags [43]. Slag 1 is additive free, the compositions of the different slags are given in Table 8.

For a melt containing only FeO and Fe_2O_3 (without SiO_2) the presence of CaO lowered the activity coefficient of Fe_2O_3 and raised the activity coefficient of FeO at high Fe_2O_3 contents, although it has no significant effect at low contents of Fe_2O_3 [43].

2.2 Ferrous - Calcium – Silicate (FCS) Molten Slags

Yazawa et al. [44] studied the possibility of using ferrous-calcium-silicate slag for copper smelting and converting. The composition of FCS slag is located on the tie line between FeO_x and calcium silicate in the ternary FeO_x-SiO_2-CaO system. This slag has never been used (2000) as copper smelting slag because of high sulfidic copper solubility, but when the dissolved copper in slag is only in oxide form this slag is quite attractive and can be regarded as the third copper smelting slag after fayalite and calcium ferrite slags [44]. According to the authors, oxidic copper loss in this type of slag is minimal. Despite the limited solubility of silica and a high fluidity, calcium ferrite slags are suitable for continuous converting.

2.3 Thermodynamic Analysis of Oxidic Copper Loss and Recovery in the Slag

Copper loss in the slag is usually in the form of oxides or sulfides and mechanically entrained matte or metallic inclusions. In addition to the slag production method physical properties of the slag (density, interfacial tensions and viscosity) also determine the amount of copper loss.

Copper loss in this form can be reduced by tuning the physical properties of the slag. For instance, a lower slag viscosity can be achieved by developing mechanisms to reduce the amount of magnetite and SiO_2 in the slag [14, 45].

Oxidic copper loss in FSF slags can be recovered using reductants like coke on top of the slag layer in the electric furnace. Once the molten slag is in contact with the reductant, the selective carbothermic reactions proceed with some influences from temperature and composition variations.

2.3.1 Activity and Dissolution of Copper in Ferrous-Silicate Slag

Activity of metal oxide is the driving force for the dissolution of the corresponding metal in the slag [48]. Thus, dissolution of metals in slag is enforced by the activity of the corresponding metal oxide. At low contents of the metal in the copper and of the metal oxide in the slag Henry`s law is valid [45]. Activity coefficient of metallic oxides is determined as a function of temperature, oxygen potential and slag composition. The influence of temperature on the activity coefficient is shown in Figure 15 and Figure 16 below. The influence of temperature on the activity coefficient of iron at infinite dilution in liquid copper can be expressed by equation (3) [45]:

$$\gamma_{Fe\,(l)} = e^{\frac{(9300 - 0.41 \cdot T)}{(RT)}} \tag{3}$$

where R is universal gas constant of value 1.987 $cal.K^{-1}mol^{-1}$. The solubility of copper in iron-silicate slags as a function of temperature, oxygen potential, Fe/Si ratio in the slag, and activity of copper in the metal phase has been intensively studied by many researchers. The oxygen potential has been controlled by means of CO/CO_2 gas mixtures.

Cu-Au alloys have been generally used in some equilibrium experiments in order to distinguish the true dissolved copper in the slag from entrained metal droplets. Gold being only slightly soluble in the slag is an excellent tracer for entrained copper [17]. Furthermore, by using an alloy, the solubility of copper in the slag can be determined as a function of its activity in metal phase [17].

Cu_2O has been chosen by many investigators as the best representation of dissolved copper in slags. This choice is consistent with the ionic nature of liquid silicates [17]. Dissolved copper in the cupric state (CuO) would seem to be rather negligible.

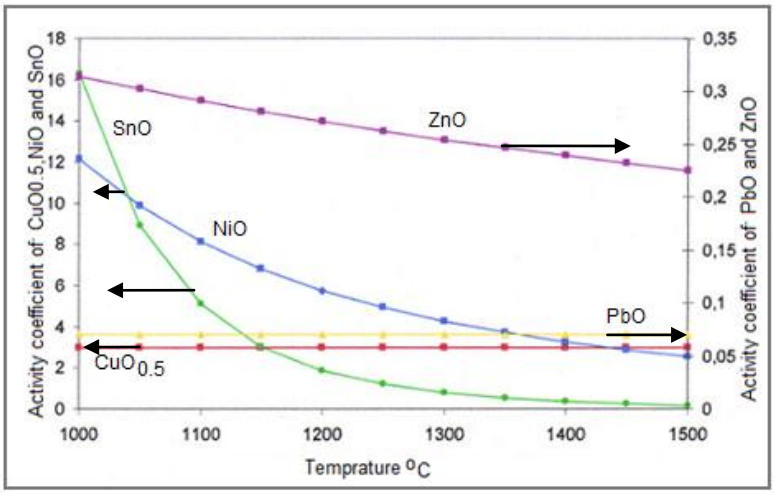

Figure 15. Activity coefficients versus temperature of metal oxides at infinite dilution in fayalitic slag (FeO-Fe_2O_3-SiO_2, where Fe/Si=1.3…5) [45, 46].

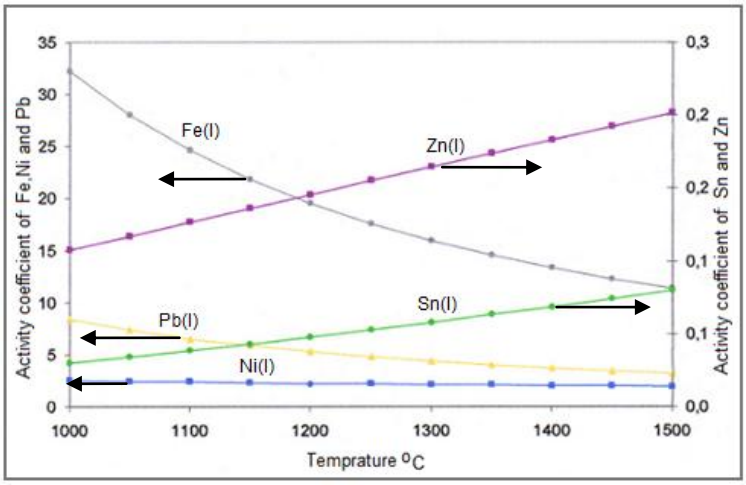

Figure 16. Activity coefficients versus temperature of several metals at infinite dilution in liquid copper [45, 46].

The solubility of copper in the slag can be represented by the following reaction:

$$2Cu(l) + 1/2O_2\,(g) = (Cu_2O)_{slag} \quad (4)$$

$$\gamma_{Cu_2O} = K\frac{(a_{Cu})^2.(P_{O_2})^{\frac{1}{2}}}{X_{Cu_2O}} \quad (5)$$

Equilibrium experiments were made to measure the copper solubility in silica-saturated iron-silicate slags containing combined and separate additions of Al_2O_3 and CaO. Results which are presented in Figure 17 revealed the fact that Al_2O_3 has a negligible effect on the solubility of copper in slags. CaO reduces copper solubility for a given oxygen pressure. MgO will also tend to reduce the solubility even though less effectively [43].

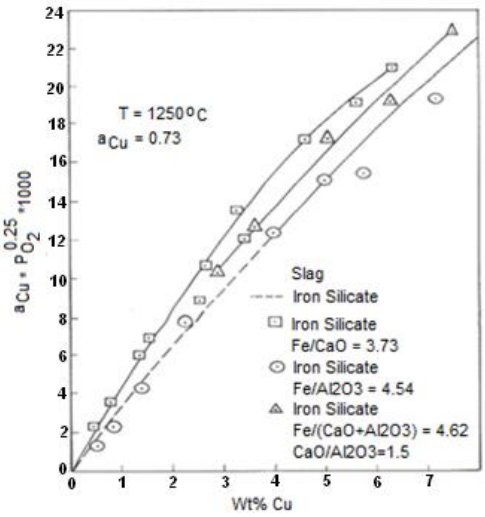

Figure 17. The effect of combined and separate additions of Al_2O_3 and CaO on the solubility of copper in iron-silicate slags [17].

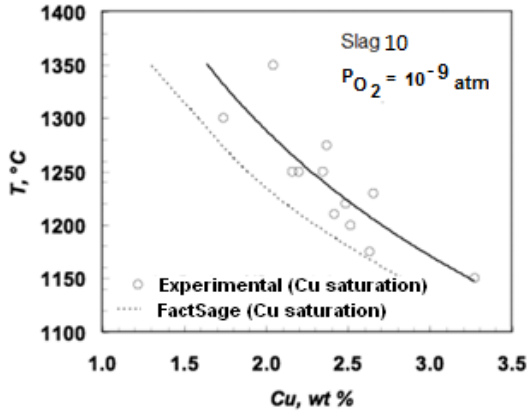

Figure 18. Copper solubility in a slag as a function of temperature along the tridymite (silica) liquidus at metallic copper saturation for the electric furnace practice and oxygen partial pressure of ~10^{-9} atm [41].

The activity coefficient of Cu_2O is very little affected by temperature or by slag composition over the wide range of Fe/Si and Fe^{3+}/Fe^{2+} ratios [17]. γ_{Cu_2O} approaches a finite value (about 2.9 for slags with a SiO_2 content ranging from 20 – 38 wt. %). As X_{Cu_2O} approaches zero, i.e., Cu_2O obeys Henry's law [17]. However, recent studies show, as indicated in Figure 18, the relationship between temperature and the extent of dissolved copper in the slag at equilibrium condition of liquid slag-tridymite and at metallic copper saturation is largely inverse [41].

This order is consistent with that of the basicity of the additive; therefore, the results can be easily expressed by the acid-base theory of the slags .The Ca^{2+}, Mg^{2+} and Al^{3+} ions would replace some of the ions, while occupying sites within the silicate structure. It is also of interest to note that this order is consistent with their similarity in radius to that of Cu^{+}, as shown in Table 9 below.

Kim et al. [43] obtained a linear relationship between the concentration of dissolved copper in slag and a_{Cu_2O} in slag. The relationship has been expressed as (for $a_{Cu_2O} \leq 0.12$):

$$[\text{wt. \% Cu}]_{slag} = Q \cdot a_{Cu_2O} \quad (6)$$

where Q is proportionality constant from which the impact of the slag additive can be measured. The value of Q decreases with the slag additives, especially with the amount of added CaO, as listed in Table 10 below. According to Diaz et al. [17] value of Q=32 can be safely used to predict the solubility of copper in iron-silicate slags in the temperature range of 1200 - 1500^{o}C, as a function of the activity of copper in the metal phase and Po_2.

Table 9. Ionic radii of ions existing in different slags [32, 43].

Ion	Ionic Radii (Å)
Cu^{+}	0.96
Na^{+}	1.02
Ca^{+2}	0.99
Mg^{+2}	0.65
Al^{+3}	0.50
Si^{+4}	0.40

Table 10. Values of proportionality constant Q (in equation (6)) by different investigators at different conditions for iron silicate slags [43]. Numbers in parenthesis represent the type of synthetic slags as listed in Table 8. *Fe/SiO2=1.5 and ** Fe/SiO2=2.0.

Investigator	Additive free	CaO	Al_2O_3	MgO	CaO + Al_2O_3	CaO + Al_2O_3 + MgO
<u>SiO_2</u>-saturated slag						
Kim et al. [43] (1250^oC)	37.7(1)	27 (2) 25.5 (5)	32.0 (3) 27.5 (6)	29 (4)	26.9 (7)	25.8 (8)
Elliot et al. [29] (1300^oC)	34.6(1)	32.1 (2) 29.3 (9) 25.7 (5)	34.2 (6)	33.7(4)	-	-
<u>SiO_2</u>-unsaturated slag						
Nagamori et al. [47] (1200^oC – 1300^oC)	-	-	27* (6) 35**(6)	-	-	-

2.3.2 High Temperature Direct Reduction of FSF Slags

In the carbothermic reaction, slag forming oxides such as silica, alumina and limestone are stable approximately up to 1650^oC (as Ellingham diagram shows, Appendix C); in contrary Cu_2O and FeO_x can be reduced at temperatures as low as 1260^oC. Therefore at low temperature selective reduction of copper and iron oxides is expected [11, 38], as shown in Figure 19. Standard Gibbs free energy changes of some reduction reactions at 1300°C are given in Appendix D. Below 1650°C direct reduction and separation of useful metals from slag making oxides into a separate liquid phase of an Fe-Cu-C alloy may be expected [11].

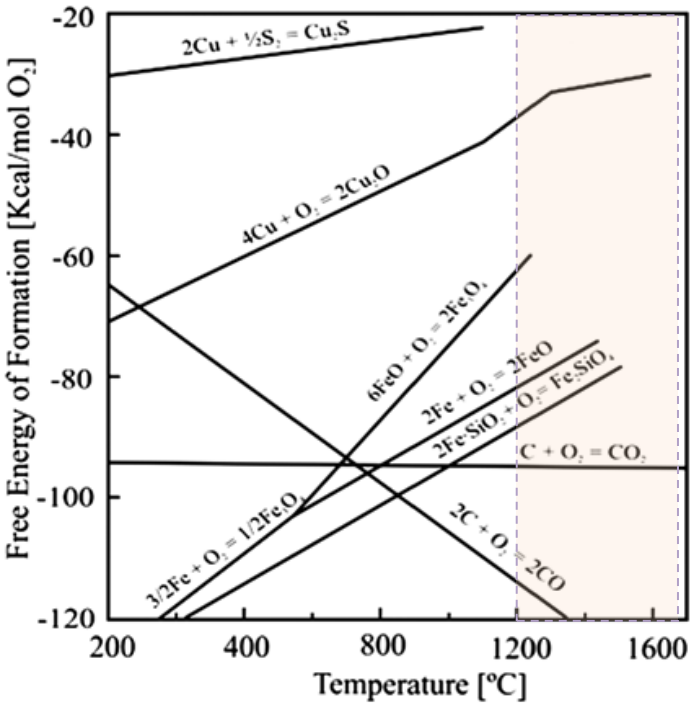

Figure 19. Free energy of formation of copper and iron oxides as a function of temperature [38].

At the presence of carbon and T > 1200^{o}C, cuprous oxide is reduced to metallic copper and magnetite is reduced to ferrous oxide and then to iron and iron silicate is also decomposed into iron, and silica according to the following reactions [11]:

$$(Cu_2O)_{slag} + C = [2Cu]_{metal} + CO\ (g) \quad (7)$$

$$(Fe_2O_3)_{slag} + C = (2FeO)_{slag} + CO\ (g) \quad (8)$$

$$(Fe_3O_4)_{slag} + C = (3FeO)_{slag} + CO\ (g) \quad (9)$$

$$(2FeO{\cdot}SiO_2)_{slag} + 2C = [2Fe]_{metal} + SiO_2(s) + 2CO\ (g) \quad (10)$$

$$(FeO)_{slag} + C = [Fe]_{metal} + CO \quad (11)$$

Reduction of the slag takes place in a series of direct and indirect reactions of the oxides with the reducing agents to form a metallic phase and gaseous products. The presence of carbon

fixes the CO/CO_2 ratio in reaction zone at a given temperature according to the following reaction:

$$CO_2\ (g) + C = 2CO\ (g) \quad (12)$$

The reduction of metallic oxides is controlled by temperature and the prevailing oxygen potential, which is fixed by the CO/CO_2 ratio in the system according to reaction below [11]:

$$2CO\ (g) + O_2\ (g) = 2CO_2\ (g) \quad (13)$$

Minor metallic oxides in the slag such as CaO, MgO and Al_2O_3 are not competing with the iron and copper oxides in the selectivity of carbon reaction. At temperature above 1260^{o}C Cu_2O can be reduced at low CO pressures compared to magnetite, which requires higher CO-partial pressure [11]. Iron silicate, where the activity of FeO is approximately 0.4 at 1260^{o}C, needs even a higher reducing condition as shown in Figure 19 [11].

2.3.3 Gibbs Free Energy Change of the Reduction Reactions

In an attempt to study conditions at which the carbothermic reactions stop or Gibbs free energy change of reactions (as expressed in equation below) turn to a positive value, an excel-program based calculation system was constructed (Appendix E). HSC Chemistry 5.11 and literature data (Table 11) were used to create a model which represents the product favored dynamic equilibrium of different reactions in copper slag cleaning processes. Temperature (1425-1773K) and activity of the slag component were the most influential variables.

$$\Delta G_{reaction} = RT(\ln\left(\frac{a_{product}}{a_{reactant}}\right) - \ln(K_p))$$

where R is universal gas constant, $a_{product}$ and $a_{reactant}$ are activities of products and reactants, respectively, and K_p is equilibrium constant of the reaction at standard conditions. As calculated results in Figure 20 show, Gibbs free energy change of the reactions studied generally increases with temperature, almost in a similar fashion. However, the reduction of ferric oxide to ferrous oxide is exceptionally radical, irrespective of the temperature change within the given range.

Table 11. Activities of the slag components (as a function of temperature) used in calculating Figure 20.

Activities of components in the slag	Assumptions and expressions	Reference
P_{co}(atm)	1 (assumption)	
P_{co2}(atm)	$(P_{CO})^2 / (K_p(T))$ (equation (12))	
P_{co2}/P_{co}	$3.5 \cdot 10^{-4}$ (T=1573K)	[49]
P_{o2}(atm)	$(5 \cdot 10^{-89}) \cdot ((T-273)^{24.129})$	[49]
a_{Cu}	-0.0013·(T-273)+2.1445	[49]
a_{Fe} (in liquid copper)	$(e^{\frac{(9300-0.41 \cdot T)}{((1.987 \text{ cal} .K-1\text{mol} -1) \cdot T)}}) \cdot$(~5wt. % Fe) (At saturation of Fe in Cu(l), i.e., $a_{Fe} \rightarrow 1$)	[45]
a_{Fe} (in the bulk slag)	$a_{FeO} / \left(K_p(T) \cdot (p_{O_2})^{1/2}\right)$	
a_{Cu_2O}	(wt. % dissolved copper in slag≈1.51)/(32)	[17]
a_{FeO}	0.35 - 0.4 (at silica saturation)	[11,13, 46, 50]
$a_{Fe_2O_3}$	$K_p(T) \cdot {a_{Fe}}^2 \cdot {P_{O_2}}^{3/2}$	
$a_{Fe_3O_4}$ (1473-1573K)	~15 wt. % Fe_3O_4 = 2.6 + 29.7a_{Fe3O4} - (10.8 - 34a_{Fe3O4})·(0.01·(T-1523)) - (2.3 - 6.7a_{Fe3O4})·(0.01·(T - 1523))^2	[13]

Ferrous oxide reduction appears to be significantly improved with temperature rise. Bar graphs of some of the important reactions at three different temperature conditions are shown in Appendix F.

The reduction of cuprous oxide is found to be thermodynamically favored over ferrous oxide reduction. Thus, at a given temperature until the concentration of Cu_2O in slag is very low copper dominates the growing and detaching metallic phases from the reductant surface. By searching the zero point of $\Delta G_{reaction}$ of equation (7) (in the constructed model) at the expense of the concentration of dissolved copper in the slag at 1573K, it has been observed that when the theoretical amount of dissolved copper in slag is less than ~2.10^{-6} wt. % there is almost no reduction of Cu_2O in the coke-slag interface. At the same temperature when Cu_2O

wt. % < 0.27, the reduction of Cu_2O in the bulk slag by ferrous oxide or iron terminates. Therefore, after this critical concentration the reduction may be considered to proceed only through the carbothermic reaction.

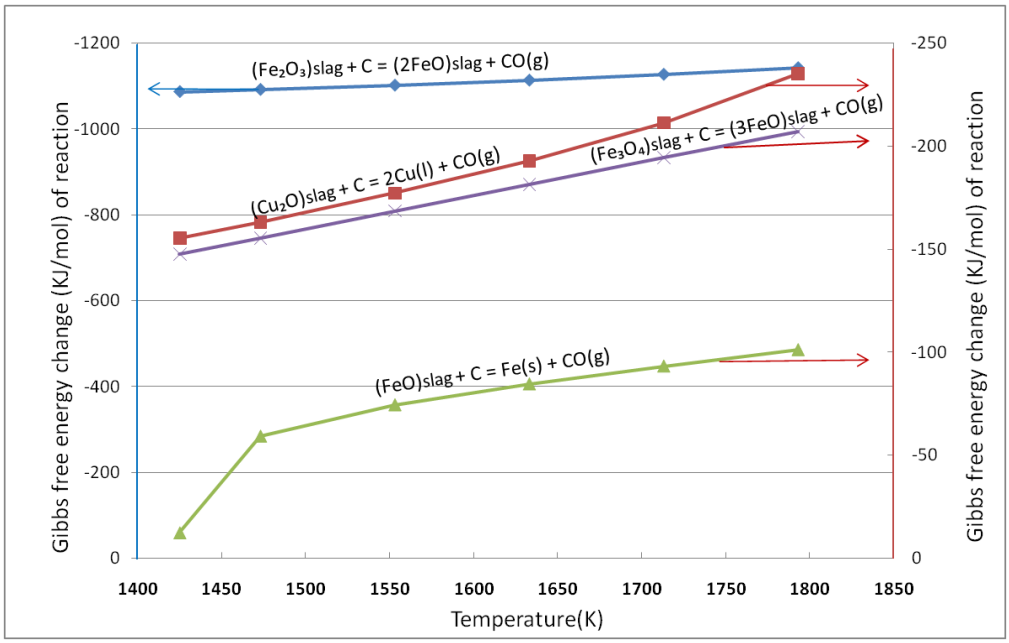

Figure 20. Calculated diagram of Gibbs free energy change of the carbothermic reactions at the slag-coke interface.

3 The Slag – Coke Interface

Comprehensive knowledge of chemical and physical kinetics at the slag-coke interface, illustrated in Figure 21, plays important role in optimizing the reduction rate of metal oxides and removal of reaction products from the interface. Surface area of the coke that is physically in contact with the slag and wetting at the interface are directly or indirectly submit to slag chemistry and temperature. Mass transfer of the reaction species to this interface, chemical reaction at the interface, and nucleation and growth of metal droplets and gas bubbles control the kinetics of metal recovery through reduction. Under intensive mixing the former has little to do with reduction kinetics. Details of reduction kinetics will be discussed in section 4.

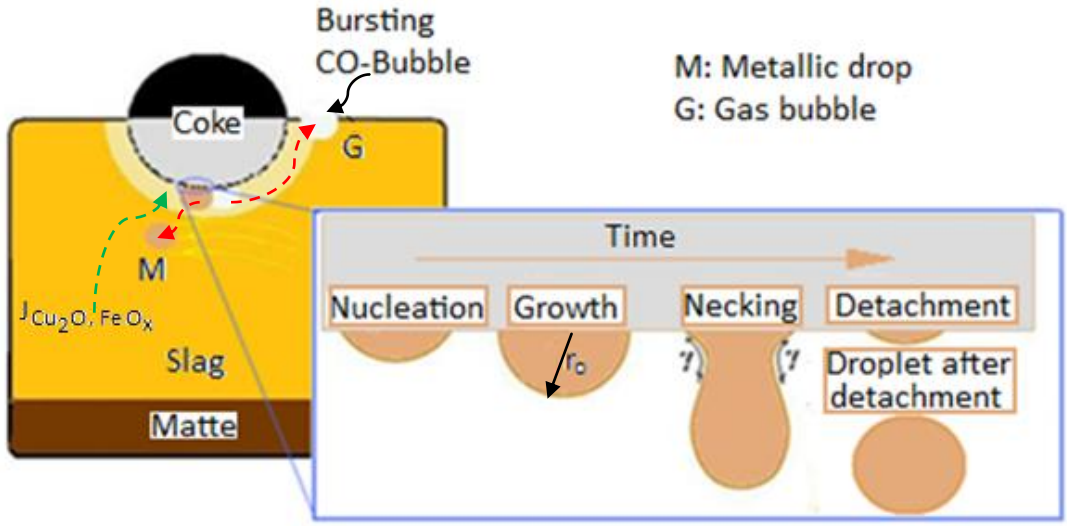

Figure 21. Schematic representation of the slag - coke interface, with magnification of a process details in the metal - coke interface.

The removal and settling/rising of the reaction products from the coke surface involves complex physical phenomena. Knowledge of interfacial tensions, density and viscosity of the materials at the high temperature enable the estimation of critical sizes and settling/rising rates.

3.1 Reaction Surface Area and Wetting Phenomenon at the Slag-Coke Interface

As mentioned earlier pyrometallurgical slag cleaning in an electric furnace involves reduction of the liquid slag using coke. The rate of reaction is proportional to the surface area of the coke exposed to the slag. As the density of coke is less than that of molten slag the coke is expected to partially submerge. This available surface area for reaction can be estimated from the Archimedes principle as follows:

$$\rho_{slag} V'_{coke} g = \rho_{coke} V_{coke} g \quad (14)$$

where V'_{coke} is the volume of the displaced slag by the submerged part of the coke. Considering a spherical coke particle and simplifying equation (14) the surface area of a coke which is available for reaction can be calculated from obtained V'_{coke} value, using the ball segment surface area (S) and volume (V) formulas below [51]:

$$V = \pi h^2 (r - \frac{h}{3}) \, , S = 2\pi r h \tag{15}$$

where h is the height of the segment as shown in Figure 22 (a).By equating V'_{coke} with the segment's volume, the value of h (r, ρ) is determined for partial surface area (S) calculation of each coke. Taking the regular arrangement of circles with the highest density, the hexagonal packing arrangement, as shown in Figure 22 (b), the number of cokes in square meter of slag surface area (N_k) is estimated and used in the cumulative surface area calculations (i.e. $N_k \cdot S$), as listed in Table 12 with the corresponding densities of the slag. It can be seen that density is the major parameter to determine the slag-coke interface area.

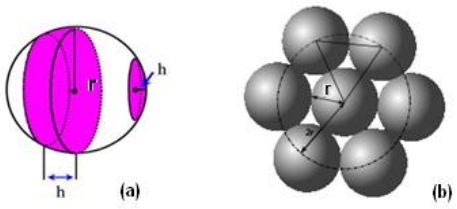

Figure 22. (a) A ball segment with segment height h and radius r (b) circles arranged in a hexagonal lattice and each circle is surrounded by 6 other circles. The surface density of this circle packing arrangement is about 0.9069 [32].

Table 12. Cumulative surface area of spherical cokes per square meter of the slag surface, as function of density of the slag at a fixed coke density of 0.95 g/cm^3.

Radius of Coke (cm) →	1	1.5	2	2.5
ρ_{slag} ($\frac{g}{cm^3}$)	Reaction surface area (m^2) per square meter of slag surface			
2.8	1.42	1.42	1.42	1.42
3	1.36	1.36	1.36	1.36
3.2	1.31	1.31	1.31	1.31
3.4	1.26	1.26	1.26	1.26
3.6	1.22	1.22	1.22	1.22

There should be good wetting between the coke surface and the liquid slag for a suitable contact so that the reaction to take place. Bhoi et al. [28] studied the wettability of graphite by CaO-SiO_2-FeO slag using the Sessile Drop technique. It was observed that the FeO content in the slag and temperature are two important factors influencing the wettability. Studying the wetting of coke by lead silicate melts in a temperature range 800-1200^oC , Heyes et al. [52] concluded complete wetting to take place for slags having surface tensions approximately below 0.2J/m^2. Thus, surface tension of the slags itself is another factor influencing the wettability.

Considering the chemical wetting, energy from chemical reactions is the driving force for a decrease in the liquid-solid interfacial tension and therefore for improved wetting [28].The contact angle θ is an accepted measure of wettability in relation to a liquid droplet on a solid surface [28, 27].

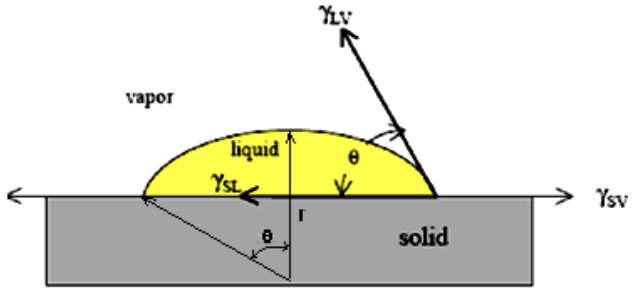

Figure 23. Contact angle and surface tension as related by Young's equation.

For a non reactive system balance of surface tension forces, shown in Figure 23, constitutes the Young equation as expressed in equation (16).

$$\gamma_{SV} - \gamma_{Sl} = \gamma_{lV}\cos\theta \qquad (16)$$

where γ_{SV} , γ_{Sl} and γ_{lV} are the surface tensions for the solid-vapor, solid-liquid and liquid-vapor interfaces, respectively. $\gamma_{lV}\cos\theta$ is accepted as the measure of wettability, and a value of this parameter between $0 < \theta < 90^o$ indicates the system to be wetting[27, 28]. When a reaction occurs at the interface, the free energy change per unit area per time also changes wetting. In this case the Young's equation (equation (16)) should be corrected for this driving force. The smallest contact angle possible in reactive system is given by [27, 28]:

$$\cos\theta_{min} = \cos\theta_o - \frac{\Delta\gamma_r}{\gamma_{IV}} - \frac{\Delta G_r}{\gamma_{IV}} \quad (17)$$

where θ_0 is the contact angle of the liquid on the substrate in the no reaction condition; $\Delta\gamma_r$, takes into account the change in interfacial energies brought about by interfacial reaction, and ΔG_r is the change in free energy per unit area released by the reaction (according to equation (11)) in the immediate vicinity of the liquid-substrate interface. This indicates that ΔG_r is one of the major factors governing wetting in the reactive system. The improved wettability with high FeO percentage in the slag may be attributed to the effect of iron oxide reduction on the interfacial energies owing to the reduction reaction [28].

According to Bhoi et al. [28] study results show, the effect of FeO on the wettability of the slag graphite interface is influenced by the amount of FeO in the slag. This effect has been shown to be more relevant for the amount of FeO in the slag is less than 20 wt. %. For over 20 wt. % (up to 40 wt. %) wettability was shown to be higher and stable. The roughness of the solid-liquid surface is an important factor in the study of slags wettability by carbon [28].

The effect of temperature on wettability is shown in Figure 24, which represents contact angle values for a temperature range between 1300 - 1600^{o}C. As the plot illustrates, temperature rise decreases the contact angle thereby increasing wettability. Increase of temperature improves the reaction rate and decreases the surface tension of the slag, which both lead to an improved wettability [28].

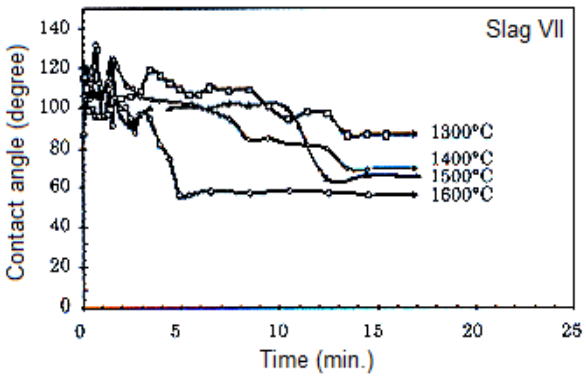

Figure 24. Variation of contact angle between Slag VII and graphite as a function of time, at different temperatures [28].

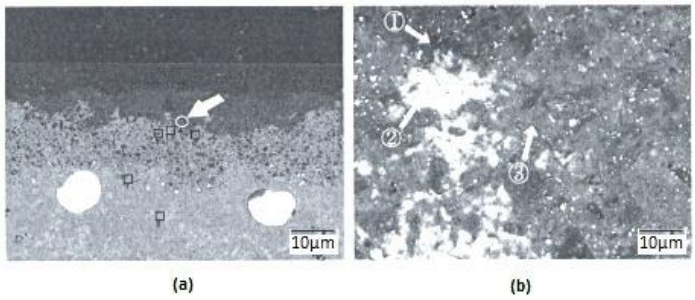

Figure 25. (a) Field Emission Scanning Electron Microscopy (FESEM) image of slag-coke interface after 135 min interaction at 1500°C, (b) magnification of circular region indicated by the arrow in (a).In (a) the upper dark black region indicates coke phase, the lower gray region indicates slag phase and the intermediate layer indicates the reacted phases [53]. EDS analysis for numbered circles are shown in Figure 26.

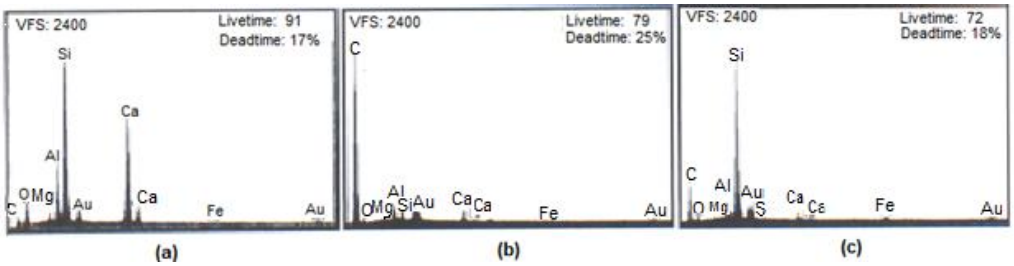

Figure 26. Energy-Dispersive X-Ray Spectroscopy (EDS) composition of white regions in Figure 25 (b) (point (1)) indicates typical bulk composition of slag droplet, (b) black zones in Figure 25 (b) (point(2)) representing typical carbon rich coke phase, (c) gray regions in Figure 25 (b) (point (3)) possibly representing the presence of SiC [53].

Sushil G. et al [53] studied the effect of composition on wetting of metallurgical cokes with different synthetic slags which resemble the typical blast furnace slags at 1500°C. As a result of CO-CO_2 gas analyzer and SEM/EDS/EPMA examinations of the coke-slag interface, as shown in Figures 25 & 26, it has been concluded that wettability of coke was strongly affected by the basicity of the slags (CaO/SiO_2= 1…1.6). More silica in the slag enhanced the wetting propensity of slags. That is, wetting at the slag-coke interface is strongly related to the kinetics of silica reduction at the interface [53].

3.2 Mass Transfer of Metal Oxides from Slag to Slag - Coke Interface

Equilibrium composition of slags and their dissolved metallic content and other coexisting phases such as gas phases and matte can be predicted by thermodynamic calculations, based on thermodynamic data available. However, thermodynamics does not help in predicting the time necessary for an equilibrium state to be reached. As a matter of fact, thermodynamics does not consider the way in which a system reaches equilibrium. Studying problems involved in the manner and rate of approach to the equilibrium state requires different method. Chemical kinetics and mass transport phenomena are the useful tools in this respect.

Chemical reactions between components of different phases take place in several steps which include the actual chemical step, which involves the breaking and making of bonds at the interface, and the transport of reactants and products to and from the reaction interface. The slow step in this sequence of steps will be the rate determining one [17].

Chemical kinetics studies the rate at which the actual chemical step occurs. Knowledge of the chemical kinetics of heterogeneous pyrometallurgical reactions is still insufficient. It is assumed that the well-established principles of collision and activation energy that govern the kinetics of a homogenous gas reaction are equally applicable to reactions between melts [17]. According to an Arrhenius equation, it is known that the rate of a homogenous gas reaction increases exponentially with temperature. Therefore, at the temperatures prevailing in copper smelting processes, reactions between chemical species are probably so rapid that the overall rate of a reaction is seldom chemically controlled [17].

The rate of most heterogeneous pyrometallurgical reactions is controlled by the transport of substances to or from the reaction zone. The principal mechanisms thereby involved are: Molecular diffusion, which results from the tendency of chemical species to move under the influence of chemical potential gradients (concentration gradients in a single phase) and bulk motion of the liquid phases, as a consequence of temperature gradients and/or stirring. The combined effect of these two is called mass transfer.

In a stagnant single phase system, the flux of a diffusing substance across a plane of unit area, perpendicular to the direction of diffusion, is given by Fick's first law:

$$J = -D\nabla C \tag{18}$$

where J is the flux, ∇C $(\frac{\partial C}{\partial X}\hat{\imath} + \frac{\partial C}{\partial Y}\hat{\jmath} + \frac{\partial C}{\partial Z}\hat{z})$ is the concentration gradient along the direction of diffusion and D (cm^2/s) is diffusivity. The diffusion coefficient in liquids varies with both composition and temperature. Composition is particularly important in molten silicates where the diffusivity would be expected to change markedly as the network-forming to network-breaking components ratio changes. The diffusivity-temperature relationship is given by an Arrhenius type equation, according to equation (19).

$$D = D_O \cdot e^{-E_a/RT} \tag{19}$$

where E_a is the activation energy for diffusion. Turbulent fluid flow predominates in the motion of fluid phases in most pyrometallurgical systems. Eddies contribute substantially to keep the bulk composition of the co-existing phases uniform. However, if reactions taking place at the interfaces are transport controlled, which is often the case, concentrations gradients are stabilized between interfaces and the corresponding bulk phases. Under this circumstance, the flux of either a reactant or a product between interfaces and bulk phases is given by:

$$ń = K_M \cdot A_i \cdot (C_2 - C_1) \tag{20}$$

where ń is the flux, A_i is the area of the respective interface, C_1 and C_2 are the corresponding concentrations in the bulk phases and interfaces, and K_M is proportionality factor called mass transfer coefficient [17]. The value of a mass transfer coefficient depends, among other factors, on the diffusivity of the chemical species to which K_M, in equation (20), applies. A direct proportionality exists between both coefficients when mass transfer takes place through a stagnant film of fluid at the interface. More complex relationships are established when eddies are continuously renewing portions of this film by elements of the bulk phase. As convective processes become more vigorous, eddies play a more important role in mass transfer phenomena and the influence of diffusivity on K_M decreases. In any case, the knowledge of diffusivities in pyrometallurgical systems contributes considerably a lot to the quantitative solution of mass transfer problems.

3.3 Nucleation and Growth of Metal Droplets and Gas Bubbles on the Coke Surface

Recovery of metallic values from molten slags by means of reduction involves nucleation and growth of new metallic phases, usually in an alloy form. Metallic droplets will nucleate and

grow at sites giving them a low Gibbs free energy. Thus the droplets and gas bubbles, as a result of reduction of Cu_2O (according to equation (7)) and FeO (according to equation (11)) will preferentially grow on the surface of the coke; i.e. heterogeneous nucleation is expected (See Figure 27 and equation (23)). The heterogeneous nuclei can take any shape and they often fill areas like cracks or scratches.

Thermodynamic driving force for phase change as a result of reaction can be expressed as (21) [54]:

$$\Delta G_V = \frac{\Delta\mu}{V^m} = \frac{\Delta G_{reaction}}{V^m} \tag{21}$$

where V^m is molar volume of the phase (m^3/mol) and $\Delta\mu$ is local supersaturation degree. The total local free energy change is (22) [55]:

$$\Delta G(r) = -\Delta G_V . V_o(m) r^{m+1} + \gamma . S_o(m) r^m \tag{22}$$

where value of m is 1 for plane, 2 for sphere/cube and 4 for lens disk shape nuclei; V_o and S_o are volume and surface factors, respectively. The critical radius of the nuclei is (23):

$$r^* = \frac{\gamma . S_o(m) . m}{\Delta G_V . V_o(m) . (m+1)} \tag{23}$$

Assuming the nucleation of a spherical cap, which can be illustrated as in Figure 23, the total driving force in equation 18 can be rewritten as (24) [54,55]:

$$\Delta G(r) = (-\Delta G_V . \frac{4}{3}\pi r^3 + \gamma . 4\pi r^2) . S(\theta) \tag{24}$$

where θ is the angle of wetting, as indicated in Figure 23. Therefore $S(\theta)$ is given by (25) [54]:

$$S(\theta) = \frac{(2+cos\theta).(1-cos\theta)^2}{4} \tag{25}$$

For instance, when $\theta = 30^o$ the corresponding value of S (θ) is 0.013, which implies that the energy barrier for heterogeneous nucleation is much less than for the homogenous nucleation, as shown in Figure 27. Depending on the angle of wetting, θ, the critical nucleus and thus

$\Delta G(r)$ can be significantly smaller for heterogeneous nucleation. The free energy need to form the critical radius in equation (22) is given by (26) [54]:

$$\Delta G^*_{het} = \frac{16}{3}\frac{\pi.\gamma^3}{\Delta G_V^2}.S(\theta) \tag{26}$$

Considering the nucleation of copper as spherical cap and taking the Gibbs free energy change per molar volume of equation (5) as a driving force for new phase formation and the interfacial tension of slag-coke (Table 3) as if copper-coke ($\gamma_{\text{slag}-\text{coke}} \pm 0.3N/m$), the critical radius is less than 1nm.

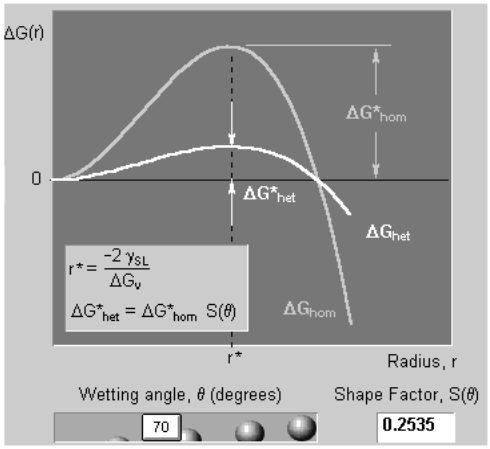

Figure 27. Diagram of total free energy vs. radius of nuclei showing the energy barrier for heterogeneous and homogenous nucleation [56].

It should be noted that the critical radius r* is the same for both homogenous and heterogeneous nucleation, as illustrated in Figure 27. However, due to the shape factor, the volume of a critical nucleus (and thus ΔG*) can be significantly smaller for heterogeneous nucleation, depending on the wetting angle θ.

Nucleation and growth of a new phase may control a reaction if the interfacial surface energies associated with the product phase are much higher than the surface energies of the interface the product displaces [24]. As listed in Table 3, gamma-iron has a surface energy of about 1.95 J/m^2 and interfacial energy of about 1.2 J/m^2 in silicate melts, and copper has a surface energy of about 1.25 J/m^2 and interfacial energy of about 0.741 J/m^2 in fayalitic slags. Thus, according

to Timothy et al. [24], nucleation and growth control of the two reactions above is less likely as the surface energies of iron and copper can be assumed larger than the slag's. If nucleation and growth is controlling, the reduction rate increases as the area or perimeter of the product increases until another process controls the reaction [24].

3.4 Kinetics of Reaction Products in the Slag – Coke Interface

A drop hanging freely in a gas phase will detach itself from a tip when its weight just exceeds the surface energy acting at its periphery. According to Tate's law the equilibrium state of this phenomenon can be written as equation (27) [57, 58].

$$2\pi\gamma r_o \sin(\Theta) - V\rho g = 0 \tag{27}$$

Based on equation (27) and taking in to account the non-stagnant nature of molten slags in an electric furnace, the size of metallic droplet that can detach from the coke surface or completes spherical shape in the slag phase can be estimated.

In the non-stagnant liquid the left side of equation (27) should be different from zero. For external forces which tend to pull down the pendant metallic drop, the difference between the two forces on the left side of equation (27) should be positive value, that is; there exists some force acting downward with the weight of the drop to overcome the interfacial energy and buoyancy force to cause earlier detachment than equation (27) predicts. This can be expressed as equation (28) below.

$$2\pi\gamma r_o \sin(\theta) - V(\rho_{Cu} - \rho_{slag})g - F_{ext} = 0 \tag{28}$$

Using values of density of copper (7600 kg/m^3) and slag (3300kg/m^3) from Table 5 and interfacial tension from Table 3, wetting angle of the slag-coke interface to be about 85^o (Figure 24) and the critical radius obtained using equation (27) (e.i., ~5mm) as the upper limit (r_o = 5000..0µm) a curve indicating the force as a function of radius was drawn. From a positive sloped tangential fitting of this curve (i.e., $F_{ext}(r_o)$ from; $[2\pi\gamma r_o \sin(\Theta) - V(\rho_{Cu}-\rho_{slag})g]$ vs. $[r_o(\sim 2000\ldots 0\mu m)]$ curve) the external force in question was estimated as a function of critical radius of the detaching drops, according to equation (29) below.

$$F_{ext} \approx -347 r_o^2 + 4.64 r_o \tag{29}$$

Equation (29) simulates 100 to 1000 times the corresponding hydrodynamic force along the y-axis in which the slag motion is about 0.1m/s. Combining equations (28) and (29), equation (30) is obtained from which the smallest possible critical radius of the detaching drop is estimated, with respect to the interfacial tension between copper drop and the slag.

$$2\pi\gamma_{Cu-slag}\, r_o \sin(\theta) - V(\rho_{Cu} - \rho_{slag})g + 347r_o^2 - 4.64r_o = 0 \qquad (30)$$

where $\gamma_{Cu-slag}$ =0.741N/m (see Table 4). Determination of critical radius from this equation is clearly by the rule of thumb and results in the curve fitting submit to the software accuracy in which this calculation was made.

To contain the effect of variables like temperature, partial pressure of oxygen and composition a wider range of interfacial tension should be considered, in this case equation (29) will also change slightly with the different interfacial tension and so do equation (30). For the interfacial tension (0.741 N/m at 1473K) the smallest critical radius of the detaching drop is (i.e., the solution of equation (30)) about 15 μm. For accurate determination of the critical size one may have to know additional forces (acting on the drop) such as; the hydrodynamic force, inertial force exerted by the continuously rising bubbles, chemical and physical forces at micro-scale and forces exerted due to the possible swinging of cokes on the molten slag layer. The critical radius estimated is in the range of values estimated (5 - 50μm) by Warczok et al. [7], even though no basis of determination is mentioned in the paper.

However, without considering the existence of external forces a hanging drop with continuous material supply for its volume to grow may segment after a certain critical volume is reached. Detachment due to the segmentation may be followed by satellite formation. This phenomenon was described by Fuchikami et al. [59]; the possible mechanisms of segmentation are illustrated in Figure 28 below.

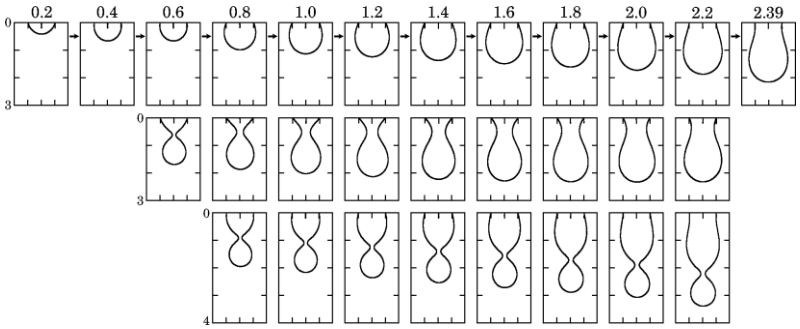

*Figure 28. Drop hanging from faucet. Various equilibrium shapes for a fixed volume of a drop. Among them, only one (the top of each column) is stable. As the volume increases, the shape changes as indicated by arrows [*59*].*

According to Suter et al. [60], the critical radius of a bubble at the onset of penetration between two liquid phases can be calculated as follows:

$$d_{bubble} = \sqrt{\frac{3\gamma_{slag-metal}}{(\rho_1+\rho_{gas})g}} \quad (31)$$

where ρ_l is density of the lighter phase and d_{bubble} is critical diameter of the penetrating bubble. According to equation (31) a small gas bubble could have a longer rest time before it penetrates into the liquid layer. The critical diameter of CO-bubble in the slag before its rise is about 8mm; it varies slightly with the density of slag as shown in Table 13.

Table 13. Critical diameter of CO-bubble variation with density of the slag $\gamma_{Cu\text{-}slag}$ = 0.741N/m.

$\rho_{slag}\ (g/cm^3)$	d_{bubble}(mm)
2.80	9.00
2.96	8.75
3.12	8.52
3.28	8.31
3.44	8.11
3.60	7.93

In the case where dynamic viscosity of the host fluid is much higher than that of the inclusion, the Stokes solution of drag force is modified according to equation (32) [10]. The rate of bubble rise and metallic drop sedimentation in a molten slag can be estimated from the relation between equations (32) and (33).

$$F_D = 3\pi d_{b/d}\mu_s v_{b/d}.\left(\frac{1+\frac{2\mu_s}{3\mu_{b/d}}}{1+\frac{\mu_s}{\mu_{b/d}}}\right) \quad (32)$$

$$F_B = \frac{4}{3}\pi\frac{d_{b/d}^3}{8}\Delta\rho g \quad (33)$$

where Δρ is absolute value of the difference between densities of slag-bubble or slag-drop in kg/m^3, F_D and F_B are the drag and buoyancy forces in N, $v_{b/d}$ is velocity of bubble or drop in m/s, and μ_s and $\mu_{b/d}$ are dynamic viscosities of slag and bubble or drop in kg.m^{-1}.s^{-1}, $d_{b/d}$ is diameter of the gas bubble or drop in m. Equating equations (32) and (33), and neglecting the ineffective viscosity of gas bubbles (~6·10^{-5} Pa.s [24]), the velocity at which the bubbles rise in a molten slag and the sedimentation rate of droplets in molten slags can be expressed as equation (34) and (35), respectively.

$$v_b = \frac{d_b^2\Delta\rho g}{12\mu_S} \approx \frac{d_b^2\rho_S g}{12\mu_S} \quad (34)$$

$$v_d = \frac{d_d^2(\rho_d-\rho_s)g}{18\mu_s}.\left(\frac{1+\frac{\mu_s}{\mu_d}}{1+\frac{2\mu_s}{3\mu_d}}\right) \quad (35)$$

Therefore, equation (35) is different from the Stokes law equation because of its consideration of the relative viscosity of inclusions, the difference is illustrated in Figure 29. Using copper FSF slags viscosity at about 1300^{o}C and interfacial tension between the slag and copper drop (from Table 3) the average rate of bubble rise (for the critical diameter calculated above) is estimated to be about 0.4 m/s, the variation of this rate with viscosity of the slag is depicted in Figure 30. Taking critical radius of a detaching drop to be 15µm, and dynamic viscosity of the slag and drop 0.3 and 0.005 kg·m^{-1}·s^{-1}, respectively, the rate at which a copper drop falls through the molten slag, according to equation (35), is about 3 µm/s. The variation of sedimentation rate of droplets according to their size is depicted in Figure 29. If there were no drops collision and then subsequent coagulation, as a result of the convection and electric

current induced stirring in the slag, the drop would have taken about 100 - 150 hours to settle to matte, which is about 1 to 1.45m below the molten slags' top layer.

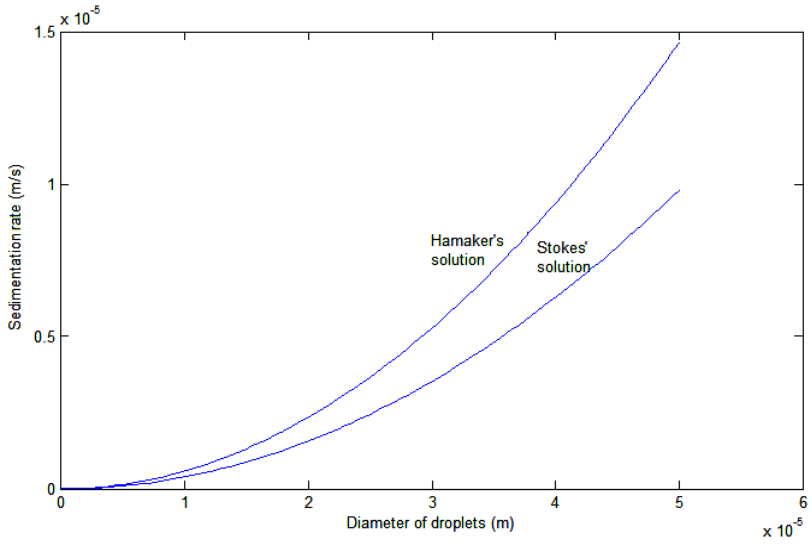

Figure 29. Calculated diagram of the settling velocity of drops as a function of their size. For comparison, the velocity of the drops calculated using the Stokes law equation (which considers droplets as solid particles) is shown.

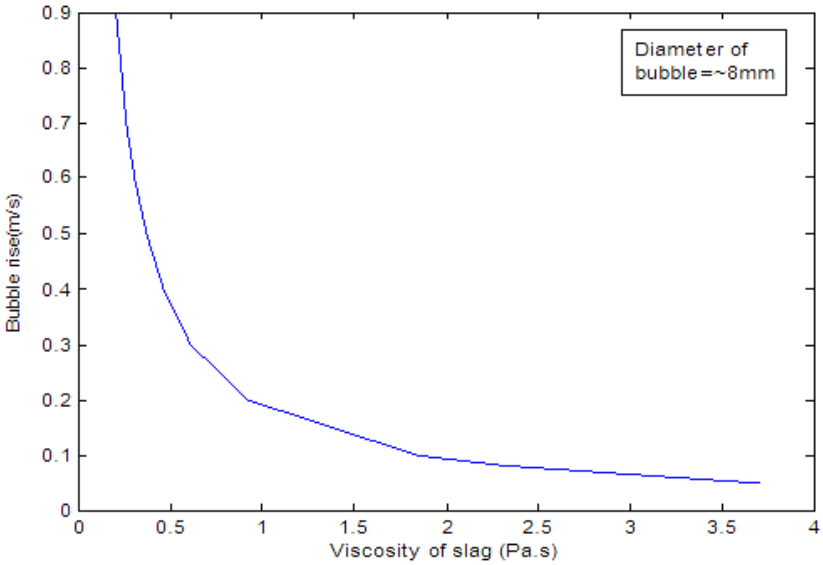

Figure 30. Calculated diagram of bubble rise as a function of slag viscosity.

4 Kinetics of Reduction

Practically any type of chemical or metallurgical reaction may be described with equation below:

$$A + B + \ldots \rightarrow C + D + \ldots, \tag{36}$$

Which involves one or more reagents (A, B, …) and results in one or more products (C, D, …). All of them might be solids, liquids, or gases. Chemistry also distinguishes between the reactions without electron transfer (e.g. ionic exchange) and with it (red-ox reactions) [61-67]. Reactions may also be realized using different mechanisms, i.e., products might be the same, but the reaction will proceed through different routes. One of the most known examples of that in metallurgy is red-ox reaction of iron. When reduction happens at higher temperatures, ferric oxide and magnetite will reduce first to ferrous oxide and then to iron.

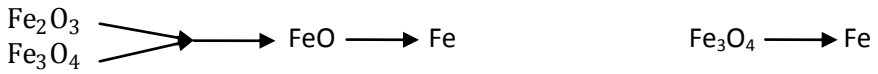

Higher temperature reduction *Lower temperature reduction where FeO is unstable*

At lower temperatures, where ferrous oxide is not anymore stable, reduction of magnetite will go directly to metallic iron. So in both cases final product is iron, but it was obtained via different routes. When analyzing kinetics of any process, one should take the difference between the "kinetics" of the reaction(s), "kinetics of the process" and "mechanism" of them. Kinetics answers the question, how fast a specific reaction or process would proceed in certain conditions. It does not consider explicitly the way or mechanism the particular process is going. Formal kinetic analyses of starting and final compositions answer the question how much the product would be generated after a certain period of time. It does not consider mechanism of reactions, neither partial reactions, if any.

Mechanism of the reaction normally involves reaction analysis on molecular level; how the species are reacting, how reagents and product transport is happening, what are the phase transformation processes, etc.

4.1 Analysis of kinetics of a Reaction

Many methods known are used for kinetic analysis and they may be classified into four categories: integral, differential, reference temperatures and multiple heating rate methods

[64-66, 68-70]. It was also reported that no single method could be recommended as superior to all others under any circumstances. When analysing kinetics of reactions from a practical point of view, a reaction model (hypothesis) is normally already set up. Here the individual reaction steps can be interpreted chemically and/or physically [64-66]. The kinetic model as a combination of individual reaction steps serves as an efficient filter for data reduction [64]. It is important that the behaviour of the test piece is investigated under conditions as close as possible to those for which the predictions have to be made. To properly extrapolate the kinetic model predictions, the largest possible range of the accessible time/temperature field [69] must be covered with isothermal measurements at different temperatures or with dynamic measurements at different heating rates to ensure the necessary level of confidence.

In a practical realisation, one may be interested in finding answer to the questions; a) how much the total reaction rate is, b) how this rate may be improved, c) what are the most limiting factors of the reaction. In general, several major limiting mechanisms are possible: by (internal) mass transport (diffusion, etc.), by the reaction kinetics itself (reaction, nucleation, catalysis), by external factors (such as heat supply), or mixed mode, where limiting factors might change in time and space. Here mostly the first two cases will be considered.

To extend the formal mechanism for other reaction types, let's formulate a reaction in the general form like (35):

$$A \rightarrow B + C \tag{37}$$

with concentration of A changing in time as [70]:

$$d\,[A]/dt = -\,U(t, T(t), [A]_o, [B], [C])) \tag{38}$$

where $[A]_o$ is concentration of starting component (for example Cu_2O in slag), [B] and [C] are concentrations of the reaction products (for example Cu and CO) and U is a conversion function. With certain limitations, for reaction (37) it is possible to apply homogeneous reactions formalism (e.g. Arrhenius theory), although this procedure is not scientifically justified [71]. It is further assumed that the conversion function U can be described by two separable functions; the rate constant k (T (t)) and the mechanism function f ([A], [B]) [64]:

$$U(t, T(t), [A],[B],[C]) = k(T(t)) \cdot f([A],[B]) \quad (39)$$

For one-step reactions, f reduces to the known form, f(α), where [A] = 1-α and [B] = α (where α is the degree of conversion with value from 0 to 1). The complete separation of variables in (39) is only possible for one-step processes [71]. For complex, multi-step processes, the differential equation (38) becomes a system of differential equations, for which a separation of variables is no longer possible. For the reaction rate constant k (T (t)), several types of the equation was suggested in the form of:

$$K(T) = K_o \cdot T^m \cdot e^{(-\frac{E_a}{RT})} \quad (40)$$

where R is the universal gas constant (8.314 J/mol·K). The exponent "m" in equation (40) depends on the consideration of the mechanism of reaction [62, 64, 71]: the collision theory predicts m = ½, the theory of the activated state predicts m = 1 and the classical Arrhenius theory (for homogeneous reactions) states m = 0. The major challenge in kinetics is thus determination of the f ([A], [B]) for a specific process, some forms of which are shown in Table 14.

This function depends strongly on the reaction mechanism. For several reactions, there might be several mechanisms (overlapping or in parallel), which makes the picture far more complicated. For example, melting is almost always a reaction of the first order where $d\alpha/dt = - A \cdot \exp(-E_a/RT) \cdot \alpha$, with α being here the degree of molten phase, but solidification can be much more complicated.

For homogeneous reactions, the kinetic equations are often fit in the n^{th} order reaction. For heterogeneous reactions it is generally understood that fitting of this type of function to kinetic data is only feasible if there are strong evidences that this is indeed the mechanism of the reaction. Here one meets the link between the mechanism and kinetic equations, one of them should be known or postulated to test different hypotheses about another one [73].

Table 14. Example of reaction types [64, 72] and corresponding reaction equations for the reaction rate $d\alpha/dt = - A \cdot \exp(-E_a/RT) \cdot f(\alpha, 1-\alpha)$.

$f(\alpha, 1-\alpha)$	Reaction type
α	1st order reaction
α^2	2nd order reaction
α^n	nth order reaction
$2 \cdot \alpha^{1/2}$	2-D phase boundary reaction
$3 \cdot \alpha^{2/3}$	3-D phase boundary reaction
$1/(2(1 - \alpha))$	1-D diffusion
$-1/\ln(\alpha)$	2-D diffusion
$3 \cdot \alpha^{1/3}(\alpha^{-1/3} - 1)/2$	3-D diffusion (*Jander's type*)
$3/(\alpha^{-1/3} - 1)/2$	3-D diffusion (*Ginstling-Brounstein type*)
$\alpha \cdot (1-\alpha)$	simple Prout-Tompkins equation
$\alpha^n \cdot (1-\alpha)^a$	expanded Prout-Tompkins equation (n, a)
$2 \cdot \alpha \cdot (-\ln(\alpha))^{1/2}$	2-D nucleation (*Avraami/Erofeev*)
$3 \cdot \alpha \cdot (-\ln(\alpha))^{2/3}$	3-D nucleation
$n \cdot \alpha \cdot (-\ln(\alpha))^{(n-1)/n}$	*n*-D nucleation/nucleus growth
$\alpha \cdot (1+K_{cat} \cdot X)$	1st order reaction with autocatalysis through the reactants (*X is a product in the model, X ~ 1-*α).
$\alpha^n \cdot (1+K_{cat} \cdot X)$	nth-order reaction with autocatalysis through the reactants

4.2 Mechanisms of Reactions

There are varieties of different reaction mechanisms. They are often based on different heat and mass transfer methods. Reaction mechanisms may consist of diffusion of one reactant through a product layer, external mass transfer (via diffusion, migration, convection etc.) in the environment, thermal diffusion (heat transfer), adsorption, absorption and desorption mechanisms. These mechanisms may change if the reactants state or condition changes. For example, if particle size of the reagent is reduced, adsorption will be improved, but heat and

mass transfer rates might be suppressed, so there will be no direct dependence of the overall reaction rate by these factors.

Most reactions in inorganic materials processing are between solids and fluids in which the solid participates as a reactant that undergoes chemical changes. Most gas-liquid and liquid-liquid reactions are rate-controlled by mass transfer, and thus their analysis reduces to a problem of mass transfer combined with chemical equilibrium at the interface. The overall fluid-solid reaction involves a combination of the following individual steps [73]:

- Transfer of the fluid reactants and the fluid products between the bulk fluid and the external surface of the solid particle.
- Diffusion of the fluid reactants and the fluid products within the pores of the solid, if the solid contains open porosity.
- Chemical reaction between the fluid reactant and the solid at the fluid-solid interface.
- Transfer of the reaction heat within the solid.
- Transfer of heat between the external surface of the solid and the surroundings by convection and radiation.
- Changes in the structure of the solid due to chemical reaction and heat.

It is known that the rate-controlling step can change depending on reaction conditions, and thus the rate information obtained under a given set of conditions may not be applicable under another set of conditions. Although this issue is well understood in scientific studies, in practical work there is often unjustified extension of the laboratory kinetic analysis onto real industrial process. Furthermore, there may not be a single rate-controlling step because several steps may have comparable effects on determining the overall rate [73]. The relative importance of these steps could also change in the course of the reaction.

Therefore, understanding how the individual reaction steps interact with each other is important in determining not only the rate-controlling step under given reaction conditions but also whether more than a single step must be considered in expressing the rate over the entire duration of the reaction.

4.2.1 Practical Analysis of the Reaction Kinetics

The kinetic analysis can be based on models which include one, two, three or more step processes in which the individual steps are linked as independent, parallel, competitive or consecutive reactions. It is assumed that all reactions are irreversible. Accordingly, in carrying out tests, this condition is “a must” to be fulfilled to the greatest extent possible. For decomposition reactions, for example, the gaseous reaction products must be removed from the reaction chamber by applying vacuum or purging with gas.

It is known that the single curve analysis of single step reactions delivers the true activation energy only when correct reaction type is used. Here, a single step reaction means a simple reaction like A → B. Today, the multivariate linear regression is selected for single step reactions and the multivariate non-linear regression for multi-step reactions [64].

If several measurements have been run on one sample at different heating rates, a model-free approximation of the activation energy can be made (Friedman, Ozawa-Flynn-Wall analysis and ASTM E698 analysis). The importance of these methods is in the ability to specify kinetic parameter and activation energy without knowledge of the specific reaction model [64-67]. Figure 31 shows an example of the Ozawa-Flynn-Wall analysis based on experimental data. It is seen that activation energy of Cu_2O reduction by carbon from slag XI (Table 18) is in the range of 185-215 kJ/mol, if this reaction is assumed to be first order reaction. However, the diagram demonstrates that first order reaction seems to be not a correct model for this process because calculated activation energy plot shows a clear dependence from the conversion degree. Thus, a more detailed analysis should be carried out.

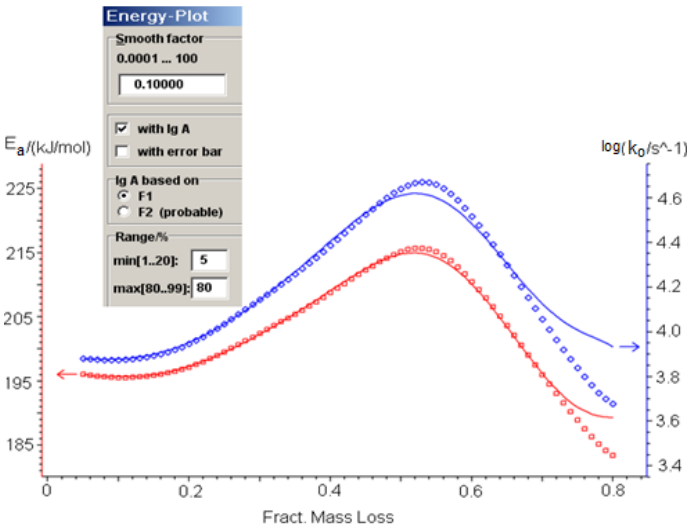

Figure 31. Ozawa-Flynn-Wall analysis of the activation energy of Cu_2O reduction by carbon from slag XI (Table 18).

4.2.2 Limitations in Formal Kinetic Analysis

Multi-step processes can be analysed with non-linear regression. It allows a direct fit of the model to the experimental data without transformation, which would distort the error structure. An additional advantage lies in the fact that there are no limitations with respect to the complexity of the model. However, only iterative procedures can be employed for estimation of the kinetic parameters.

This proves to be advantageous for one-step processes as well, because it provides a considerably better quality of fit as compared to multiple linear regressions. Since time and not temperature serves as the independent base variable in all analyses, the analyses are correct for any temperature profile. Therefore, dynamic and isothermal measurements can be combined in one analysis.

For any kind of process, one should know whether the proposed model is suitable to characterise the experiment, and, if there were many similar models, which is the most suitable. Statistic analysis of the fitting data cannot be underestimated here. This is especially true for problems in which the pairs of values follow one another (serial pairs of values), e.g. for all kinetic problems. Correlation of the least square remainders usually results in the underestimation of their variance. Therefore, for serial pairs of values, a check for auto-

correlation of the remainders should be carried out prior to performing a t-test or F-test. The most useful test for this is, that developed by Durbin et al. [74], d-test. It formulates the zero hypotheses upon the absence of auto-correlation of the remainders. Not only values of the kinetic parameters are of interest but also the extent to which the estimated parameters are statistically guaranteed. Therefore, the standard errors of the parameters have the same significance as the parameters themselves.

Most thermal measurements of a process are performed on solids and fluids, so the reaction in process cannot be observed in isolation from material and heat transfer processes, which precede or follow it. Common to all thermal measurements is that they are relatively unspecific with respect to the model or reaction type. Therefore, it is not recommended to decide about the reaction type or the kinetic model solely on the basis of a single thermal measurement. Furthermore, experience has shown that a correlation of the residues absence is seldom. Based on the measurement principle, this would be expected for thermal measurements: disturbances, which occur at the beginning of a reaction, are propagated in all of the experimental values that follow.

4.3 Reduction by Coke

Solid carbon in the form of coke or coal is used in many metallurgical processes to control the oxygen potentials of molten slags and to recover metals from solutions. Hayes et al. [52], commented on the reactions between molten metal oxides and various forms of carbon. The reactions of solid carbon with metal oxides in the slags result in the formation of gaseous carbon monoxide. A number of possible reaction mechanisms have been identified in various reaction systems. The direct reduction mechanism can be presented as equations (41) & (42).

$$(MeO)_{slag} + C \rightarrow Me(l) + CO(g) \quad (41)$$

$$(2MeO)_{slag} + C \rightarrow 2Me(l) + CO_2(g) \quad (42)$$

where Me is a metal species. These reactions require the simultaneous contact of four phases. For this reason some researchers proposed a two-stage gas ferrying mechanism involving carbon dioxide and carbon monoxide to be the possible mechanism [52]. At the presence of solid carbon, carbon dioxide produced by the reduction reaction forms carbon monoxide through the carbon gasification reaction at the coke-gas interface according to equation (12)

[52]. Kinetics of The Boudouard's reaction is given by an Arrhenuis type equation below [75] (for bituminous carbon with 20% impurity and average size of 200µm, at about 1000K):

$$\frac{d[CO_2]}{dt} = 3.13 \cdot 10^6 \cdot e^{\left(\frac{-196\,200}{RT}\right)} \cdot P_{CO_2} \quad (43)$$

The carbon monoxide gas produced is then available to react with the slag at the slag-gas interface, i.e.:

$$(MeO)_{slag} + CO(g) \rightarrow 2Me(l) + CO_2(g) \quad (44)$$

The reaction cycle is completed when the carbon dioxide returns to react once more with solid carbon. If the gasification reaction is fast compared with the slag-gas reaction, the resultant product gas should approach the carbon-gas equilibrium. If all the carbon dioxide produced is converted to carbon monoxide, then the stoichiometry of the overall reaction is identical to that of equation (41) [52].

4.4 Reduction Reactions Within the Molten Slag

The kinetics of slag-metal reactions are determined by mass transfer. This occurs in two ways: normal mass transfer which is induced by stirring and mass transfer by interfacial convection induced by interfacially active elements like oxygen and sulfur [76]. It is assumed that coupled reactions of the type as in equation below occur at the slag-metal interfaces [46].

$$M^M + 1/2\sigma(O) = (MO_\sigma)^S$$

where M^M represent the metallic components and $(MO_\sigma)^S$ the oxides dissolved in slag. In slags containing iron or other species which can exist in more than one oxidation state, electrochemical reactions involving these species can play important roles [52]. For example, the following reactions have been studied using a variety of experimental techniques from full-scale reactors to controlled laboratory experiments [52].

$$O^{2-}_{(slag)} + CO(g) \rightarrow CO_2(g) + 2^{e-} \quad (45)$$

$$2Fe^{3+}_{(slag)} + 2^{e-} \rightarrow 2Fe^{2+}_{(slag)} \quad (46)$$

$$2Fe^{2+}_{(slag)} + Me^{2+}_{(slag)} \rightarrow 2Fe^{3+}_{(slag)} + Me^{O}_{(l)} \quad (47)$$

Reduction reactions in slag bath may be explained by the recovery of metals at the absence of any added reagents. Prabhu et al. [2] studied the extent of the internal reduction of Cu_2O in slag XII (Table 18) at 1573K. As Figure 32 shows, copper recovery started lately, and increased and stabilized to far less extent than the case where carbon was used as a reagent. This is in agreement with earlier results from the thermodynamic analysis (Appendix F). The reduction of Cu_2O may proceed by the following reactions:

$$Cu_2O + 2FeO_{(slag)} = 2Cu_{(l)} + Fe_2O_{3(slag)} \quad (48)$$

$$Fe_{(s)} + Cu_2O = 2Cu(l) + FeO_{(slag)} \quad (49)$$

$$3FeO_{(slag)} + Cu_2O_{(slag)} = Fe_3O_{4(slag)} + 2Cu_{(l)} \quad (50)$$

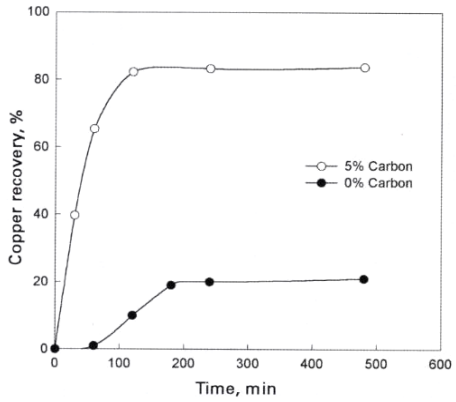

Figure 32. Copper recovery from slag XII (Table 18) at 1573K as a function of time, with and without carbon addition [2].

4.5 Reduction Rate of FeO_x

Most of chemical kinetic studies on the reduction rate of iron oxides are conducted based on steel making slags of high binary basicity (B= CaO/SiO_2). The use of experimental data concerning the reduction rate of iron oxides from these slags to optimize the reduction rate of iron oxides from slags of low basicity is difficult to reconcile, at least as activation energies of the reactions are prone to the basicity differences. In a rare event, Vartiainen et al. [13] conducted an experiment to study the reduction rate of iron oxide from fayalite-type slags

using graphite. The experiment was done in a temperature range of 1250 -1400^{o}C with different Fe/Si mass ratios, $[Cu_2O]_o$ and $[CaO]_o$. The reaction rate constants obtained in the experiment at various conditions are listed in Table 16.

As a result of the experiment, it has been reported that the carbothermic reactions started immediately when the molten slag is in contact with the reductant. The reduction of ferric oxide (Fe^{+3}) to ferrous oxide (Fe^{+2}) takes place first [13], consistently with earlier results of thermodynamic analysis.

The experimental study in which the graphite rod rotates 12 revolutions per minute, suggested that the reaction at the slag-graphite interface is the rate limiting step. However in some experiments it has been observed high CO concentration in gas phase, where its amount reduced significantly in time and CO_2 amount increased.

Table 15. Instantaneous, natural logarithmic and inverse value of $[Fe_2O_3]$ in slag of composition: $[CaO]_o$ = 10.32, Fe/Si (mass ratio) = 3.08, $[Cu_2O]_o$ = 2; while carbothermic reaction at 1300^{o}C [13].

	0-order test	1st-order test	2nd-order test
t(s)	$[Fe_2O_3]$	$\ln([Fe_2O_3])$	$1/[Fe_2O_3]$
0	22.5	3.11	0.04
1000	21.5	3.07	0.05
2000	18.5	2.92	0.05
3000	17.5	2.86	0.06
4000	16.0	2.77	0.06
5000	14.9	2.70	0.07

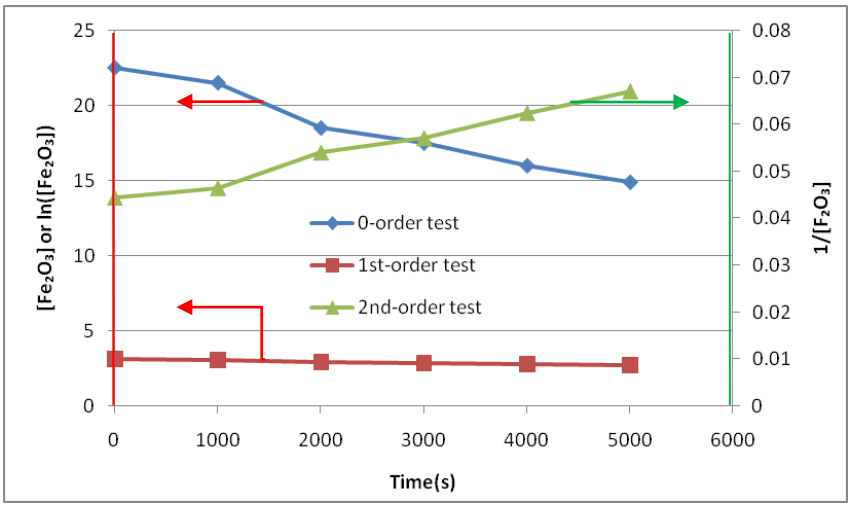

Figure 33. Concentration, its logarithmic and inverse value versus time of ferric oxide in slag described in Table 15 while reducing to ferrous oxide by carbon at 1573 K.

As Figure 33 shows only $\ln[Fe_2O_3]$ vs. time curve is linear, which implies that the reduction of ferric oxide by carbon to be the first order with respect to its concentration, consistent with the author's conclusion.

The reduction rate of metal oxides from liquid synthetic slags of similar compositions to that of fayalite-type slags by carbon was also studied by Warczok et al. [77]. They proposed the reduction reaction to proceed via an indirect reduction process and the Boudouard reaction. Based on the results of activation energy obtained in the study, it has been reported the rate limiting step in the magnetite reduction is the Bouduoard reaction (equation (12)). Activation energies of some of the carbothermic reactions estimated by different authors are listed in Table 17. The reduction rate of magnetite (as shown in Table 17) was found to be of first order with respect to its concentration and represented by equation (51) below [12, 77]:

$$\frac{d[Fe_3O_4]}{dt} = \left(8.10^3 (m \cdot s^{-1}) \cdot e^{-\frac{232000}{RT}}\right) \cdot \frac{A_r \rho_s}{m_s} \cdot [Fe_3O_4] \qquad (51)$$

where ρ_s and m_s are density (kg/m^3) and mass (kg) of the slag, respectively. The rate determining step in the reduction of ferrous oxide to Fe^o would change from the mass transfer of FeO at low [FeO] (< 5 wt. % in slag [36]) to the chemical reaction at the reaction interface at high [FeO] [36,78], like in slag XVIII (Table 18).

Table 16. Average apparent rate constants of Fe_2O_3 reduction by carbon at different temperature and composition of slags [13].

Composition (wt. %)			Temperature(^{o}C)		
Cu_2O	CaO	Fe/Si(mass ratio)	1250	1300	1400
			$k \cdot 10^4$ (Numbers in bracket indicate the time range (s) in which the rate constants are calculated)		
0	0	3.40	1.89(300-1530)		
	0	4.56	1.61(300-2280)		
	0	2.88		3.07(480-3000)	
	0	3.76		4.62(225-1500)	
	0	3.76		1.87(240-2700)	
	0	3.76		3.25(150-1800)	
	0	3.96			5.08(30-720)
	5	3.33	1.85(180-1980)		
	5.08	4.48	1.41(660-2340)		
	5.25	3.36		2.23(120-2220)	
	5.27	4.40		1.88(360-3600)	
	8.45	3.81		2.06(390-1800)	
	9	3.30	1.89(60-1680)		
	9.89	4.40	1.58(900-1920)		
	10.32	3.07		3.32(600-1200)	
1	0	3.40	2.22(180-1320)		
	0	4.56	1.97(390-1500)		
	5	3.33	2.12(510-2400)		
	5.08	4.48	1.93(480-1800)		
	9.45	3.01	2.14(90-2430)		
	9.89	4.40	1.79(300-1800)		
2	0	2.88		3.53(240-3000)	
	0	3.40	2.14(360-2400)		
	0	3.40	2.59(840-3030)		
	0	4.12		3.66(180-1800)	
	0	4.56	1.81(180-1800)		
	5	3.33	2.28(660-1740)		
	5.08	4.48	1.76(600-1980)		
	5.25	3.36		4.11(180-600)	
	8.45	3.81		4.08(120-1500)	
	9.98	3.30	2.07(600-3060)		
	9.89	4.40	1.17(600-5040)		
	10.32	3.07		1.00(180-3015)	
4	0	2.88		3.05(120-2520)	
	0	4.12		6.88(210-1020)	
	5.25	3.36		3.66(300-720)	
	5.25	3.36		2.76(180-900)	
	5.27	4.40		1.80(210-3000)	
	8.45	3.81		1.09(300-2820)	
	10.32	3.07		5.11(150-300)	
6.0	0	3.96			8.61(210-1110)

Based on results of the study and comparisons with thermodynamic data for FeO in slag XVIII, the reduction rate of FeO (for a wide range of FeO concentration in the temperature range of 1723 - 1823K) can be expressed as equation (52) below [78]:

$$\frac{\mathrm{d}[\mathrm{FeO}]}{\mathrm{dt}} = 1.67 \cdot 10^{-7} \cdot [\mathrm{FeO}]^{1.26} \quad (52)$$

The rate of FeO reduction from the slag at different initial concentrations is illustrated in Figure 34 below. However, the temperature range of the study is far beyond the conventional temperature range in the FSF slag cleaning processes. Unfortunately, the reduction rate of FeO by carbon from slags resembling copper FSF slags under the condition of the slag cleaning processes is not seen in publications. It might be considered that the final stage $Fe^{+2} \rightarrow Fe^{o}$ does not play a significant role in the copper reduction from these slags at lower temperatures, at least before Cu^{+} is reduced significantly.

Table 17. Activation energy of some of important reactions in the slag cleaning process. The slag compositions are given in Table 18.

Reaction	Activation energy (kJ/mol)	Temperature(k)	Composition [Ref.]
$(Cu_2O)_{slag} + C = [2Cu]_{metal} + CO$	188.4	1513-1598	Slag XI [1]
$CO_2(g) + C = 2CO(g)$	246.8	973-1673	[1]
$(Cu_2O)_{slag} + C = [2Cu]_{metal} + CO$	175	1513-1613	Slag XII [2]
$(Fe_3O_4)_{slag} + CO = (FeO)_{slag} + CO_2(g)$	232	-	Slag XIX [7]
	230	1523	Slag XIX [12]
$(Cu_2O)_{slag} + C = [2Cu]_{metal} + CO(g)$	206.20 ± 10	1513-1598	Slag XI [64]
$(2Fe_2O_3)_{slag} + CO\ (g) = (2FeO)_{slag} + CO_2\ (g)$	154.4	1523-1673	Slag XIII [13]
	234.78 (based on two point slope)	1523-1573	Slag XIV [13]
$(FeO)_{slag} + C = [Fe]_{metal} + CO(g)$	251.05	1730-1800	Slag XVIII (10 wt. % FeO) [78]

Table 18. Composition of different synthetic slags used by various authors for studying the reduction rate of metal oxides using carbon as a reductant. Numbers in parenthesis are compositions in wt. % [1, 2, 7, 12, 13 , 64, 78].

Slag No.	Composition
XI	$CuO_{0.5}$(1.63)- FeO(33.97)-Fe_2O_3(6.34)-SiO_2(29.5)-CaO(18)-Al_2O_3(8.94)
XII	Cu(1.24)-Zn(1.76)-Ni,Cr,Pb & Sn(1.23)- FeO(32.1)-SiO_2(27.8)-CaO(14.6)-Al_2O_3(8.5)- MgO(2.2)
XIII	Fe/Si (mass ratio: 4 - 4.4)
XIV	Fe/Si (mass ratio: 3.33)-CaO (5)-Cu_2O (2)
XV	Fe/Si (mass ratio: 3.07)-CaO(10.32)-Cu_2O (2)
XVI	Fe(35-42)- SiO_2 (26-28)- Fe_3O_4 (17-22)- Cu(6-10)- Cu(Dissolved)(0,5-3)-Cu(Matte Inclusions)(4-8)-Cu(Metallic Copper Inclusions) (0,5-1)- S(1.5-2.5)- CaO (1-1,5)
XVII	FeO(37)-SiO_2(38)-CaO(2.6)- Al_2O_3 (7.3)- Fe_3O_4(8)-Cu (0.05)- MgO(2)-Ni(0.24)-Co(0.07) (Total Fe(34.4))
XVIII	FeO(1-70)-Fe_2O_3-Al_2O_3(5)-CaO-SiO_2(CaO/SiO_2=1.15)
XIX	Fe(35-42)-Cu(6-10(0.5-3 dissolved))-S(1.5-2.5)-Fe_3O_4(17-22)-SiO_2(26-28)-CaO(1-1.5)

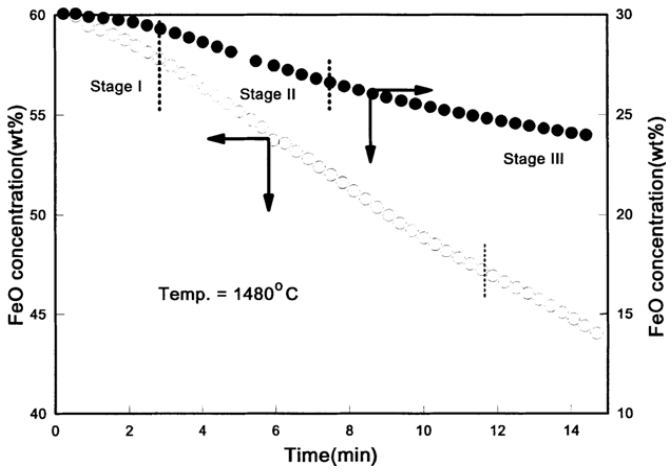

Figure 34. FeO concentration change in slag XVIII with time [78].Stage I: Incubation period with nucleation and growth of generated gas, Stage II: A steady-state reaction region in proceeding reaction with gas film, stage III: A degradation period by local deficiency of FeO at the gas/slag interface [78].

4.6 Reduction Rate of Cu_2O

The variation of concentration of dissolved cuprous oxide in slag XI (Table 18) as a result of its reaction with graphite was experimentally studied by Reddy et al. [1]. The arrangement of the experiment is shown in Figure 35 below:

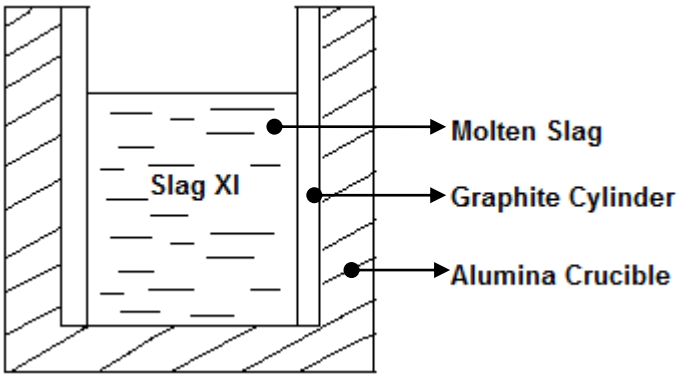

Figure 35. Schematic diagram of the alumina crucible filled with molten slag in the experiment [1].

As a result of the experiment, it has been concluded that at any given temperature the amount of cuprous oxide present in the slag falls rapidly and reaches a steady state value. The rate of reduction of the oxide increased with increasing temperature [2], as suggested by the thermodynamic analysis in section 2.3. The concentration of copper in slag XI (Table 18) falls from the initial content of 1.24 wt. % to about 0.2 wt. % after 2 hours of the reduction process [1]. Approximation of data [1] using formal kinetic analysis in equations (36-40) and Table 14 leads to the following equation (53), describing this reduction process as an autocatalytic reaction [64]:

$$\frac{d[Cu_2O]}{dt} = -k_o \cdot e^{\frac{-E_a}{RT}} \cdot [Cu_2O] \cdot (1 + k_{cat} \cdot [Cu]) \quad (53)$$

where K_{cat} is the autocatalytic coefficient and its value is given in Figure 36. Here $[Cu_2O]$ was normalized to $[Cu_2O]_o$ as unity, $[Cu_2O] = \frac{[Cu_2O]_t}{[Cu_2O]_o}$ and [Cu] =1 - $[Cu_2O]$. Unfortunately, the data by Reddy et al. [1] do not contain iron reduction values and thus it is not possible to estimate whether metallic copper or iron is the main reason for the autocatalytic behavior. The effect of temperature on the rate constants given by the Arrhenius relation in equation (40) yields the

activation energy of the reaction to be 206 ± 10 KJ/mol, which correlates well with the model-free analysis by Ozawa-Flynn-Wall method, as shown in Figure 31.

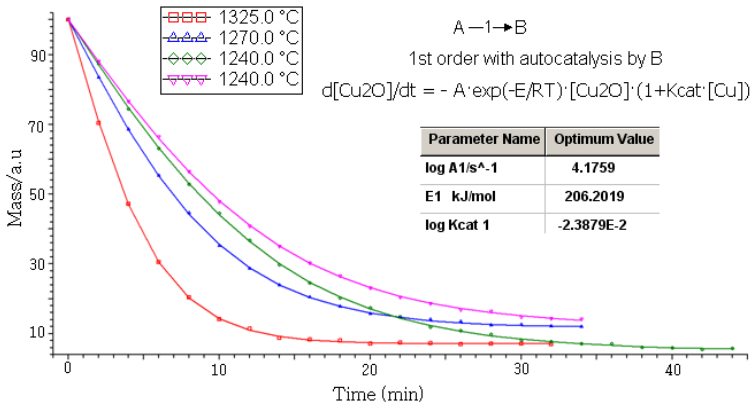

Figure 36. Plot of mass change of Cu_2O vs. time of the autocatalytic reduction reaction (in equation (7)) from slag XI (Table 18) at three different temperature conditions with one curve having a different initial composition.

Reduction of Cu_2O is controlled by the chemical reaction at the slag/graphite interface [1]. However, based on the activation energy obtained in the experiment the author in his later assessment concluded that reduction rate of Cu_2O was controlled by the Boudouard reaction catalyzed by the presence of Cu_2O. It should be, however, noted that the latter assessment was made for blast furnace slags.

4.6.1 Simultaneous Reduction Rate of FeO_x and Cu_2O

In slags containing both Fe_2O_3 and Cu_2O, the reduction reaction proceeds as follows [13]: at the first instance of the carbothermic reaction, only Fe_2O_3 is reduced until the equilibrium partial pressure of oxygen for copper saturation point is reached. After this saturation point, Cu_2O starts to be reduced. The probable reaction mechanism is according to equations (7), (8) and (12) [13].

Eventually, after a certain period cuprous oxide will be reduced simultaneously with ferric oxide in the carbothermic reaction. The reduction of ferric oxide is 1^{st} order with respect to its initial concentration [13]. Therefore, using formal kinetics formulated through equations (36) – (40) and Table 14 ferric oxide reduction rate can be expressed as:

$$\frac{\mathrm{d}[\mathrm{Fe_2O_3}]}{\mathrm{dt}} = \mathrm{k}\left(\mathrm{T}, \mathrm{CaO}, \frac{\mathrm{Fe}}{\mathrm{Si}}, \mathrm{Cu_2O}\right) \cdot [\mathrm{Fe_2O_3}] \quad (54)$$

Where the reaction rate constant of the reduction fluctuating with composition and temperature is expressed as equation (55) below, experimental value of this parameter is listed in Table 16.

$$\mathrm{k}\left(T, CaO, \frac{Fe}{Si}, Cu_2O\right) = -\mathrm{k_o} \cdot \mathrm{e}^{(-\mathrm{E_a}/\mathrm{RT})} \quad (55)$$

Even though results of the apparent rate constants of Cu_2O and Fe_2O_3 are obtained from two different experiments, the composition of the slags are nearly similar to each other (Cu_2O from slag XI and Fe_2O_3 from slag XV (see Table 18 for composition of the slags)).

Prabhu et al. [2] studied the effect of addition of CaO (up to 5 wt. % addition on top of 14.6 wt. % CaO already existed in the slag) to slag XII (Table 18). it was reported that there were no significant effects on the recovery of copper, as illustrated in Figure 37.

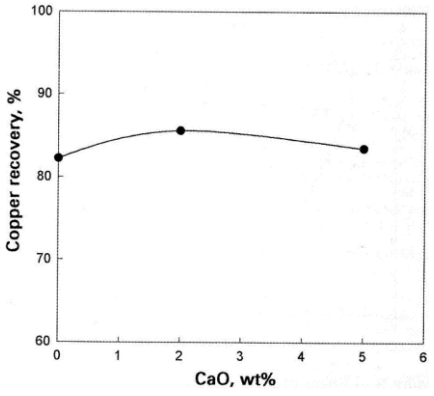

Figure 37. Effect of CaO addition on the recovery of copper from slag XII at 1573K with 5% carbon after 2 hours of reduction [2].

Thus, given the accuracy of the experimental results the calculated diagram in Figure 38 may be considered to be a representative of reduction rate of the two oxides from the same slag of basicity ~0.6. The initial amount of Cu_2O differences may be considered as if decrease in amount due to the presence of more CaO in the slag with lower $[\mathrm{Cu_2O}]_\mathrm{o}$. However, kinetics can be different when considering slag of composition listed in Table 7, where basicity is about

0.2. The effect of composition is discussed in section 4.5. A summary of the reduction rate of metal oxides from different synthetic slags is listed in Table 19.

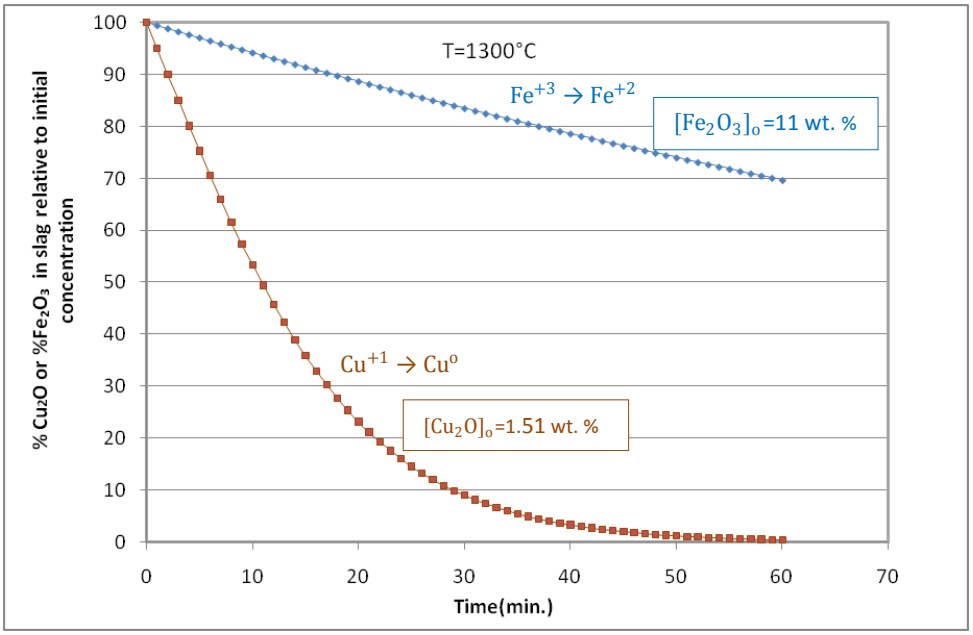

Figure 38. Estimated diagram of the rate of percentage change of the two competing metal oxides relative to their respective initial amount in slag. Calculated using the relations in equations (53) and (54).

In studying for a possible recovery of Fe from copper FSF slags, CaO-SiO_2-FeO slag system where CaO/SiO_2=1.5 was reduced by graphite rod at 1450^{o}C and the following conclusion was drawn [38]; during the first 15 minutes of the process concentration of iron remains almost constant while Cu content in the slag decreased sharply (from 2.3 wt. % to 0.5 wt. %). According to the study, iron oxide reduction started when the copper content in the slag was stabilized. This is because the thermodynamic stability of FeO is relatively high, which implies the processes is selectively dropped in the first phase of the reduction process where Cu_2O and Fe_2O_3 are abundant relative to their respective initial concentration. The Cu_2O reduction rate achievements illustrated by Dusan et al. [38] well agree with the reduction rate presented by Reddy et al. [1] even though the temperature and basicity differences are wide.

Table 19. Summary of the reduction rates of metal oxides by carbon from slags similar to the copper FSF slags. Slag compositions are given in Table 18.

Reaction	Reduction rate	Composition [Ref.]
$(Fe_3O_4)_{slag}$ + CO(g) = $(FeO)_{slag}$ + CO_2(g)	$\frac{d[Fe_3O_4]}{dt} = k(\frac{m}{s}) \cdot \frac{A_r \rho_s}{m_s} \cdot [Fe_3O_4]$	Slag XVI [7]
Fayalite slag reaction with carbon	$\text{Rate}\left(\frac{\text{mol O}}{m^2 s}\right) = 4 \cdot 10^6 \cdot (1 + \frac{[Fe_3O_4]}{15}) \cdot e^{\frac{-29600}{T(k)}}$	Slag XVII [79]
	$\text{Rate}\left(\frac{\text{mol O}}{m^2 s}\right) = 5.39 \cdot 10^6 \cdot e^{\frac{-29600}{T(k)}}$	Slag XVII [79]
$(FeO)_{slag}$ + C = $[Fe]_{metal}$ + CO(g)	$\text{Rate}(\frac{\text{mol FeO}}{(cm^2 s)}) = 1.67 \cdot 10^{-7} \cdot [FeO]^{1.26}$	Slag XVIII [78]
$(2Cu_2O)_{slag}$ + C = $2[Cu]_{metal}$ + CO(g)	$\frac{d[Cu_2O]}{dt} = -k_o \cdot e^{\frac{-E_a}{RT}} \cdot \frac{[Cu_2O]_t}{[Cu_2O]_o} \cdot \left(1 + k_{cat} \cdot \left(1 - \frac{[Cu_2O]_t}{[Cu_2O]_o}\right)\right)$	Slag XI [64]
$(Fe_2O_3)_{slag}$ + C = $(2FeO)_{slag}$ + CO (g)	$\frac{d[Fe_2O_3]}{dt} = k\left(T, CaO, \frac{Fe}{Si}, Cu_2O\right) \cdot [Fe_2O_3]$	Slag (Table 16)[13]

As results in Figures 36 & 39 show, the reduction rate of cuprous oxide can be divided into three different stages: 1) when the rate curve plunges down in to the plateau region, 2) the plateau region and 3) after the plateau region in which the reduction rate slightly decreases with the small scale concentration fall.

4.7 Effect of Temperature and Composition

The effect of temperature on the rate constants follows the Arrhenius type equation given in equation (40). A study on the reduction rate of Cu_2O using graphite as a reducing agent from slag XI (Table 18) at three different temperatures revealed that temperature has a strong influence on the reaction rate [1]. The rate of reduction increased with temperature rise as illustrated in Figure 39. This effect was also reported by Vartiainen et al. [13] for the reduction rate of ferric oxide by carbon from different slag systems.

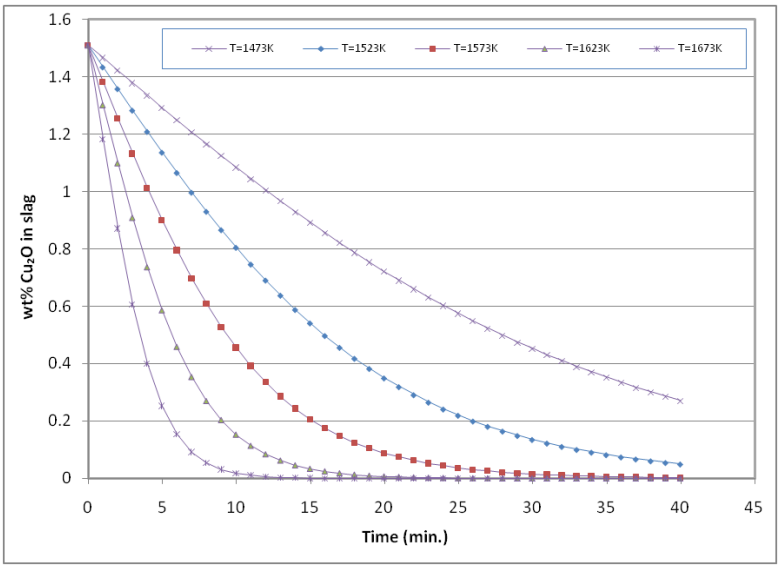

Figure 39. Estimated instantaneous amount of Cu_2O in slag as the result of the carbothermic reactions. Calculated based on relations in equation (53).

Conducting an experiment on the reduction rate of cuprous oxide at 1513K from slag XI (Table 18) as a function of initial compositions (at 1.63 wt. % Cu and 8 wt. % Cu), Reddy et al. [1] concluded that the initial concentration does not have influence on the reduction kinetics of cuprous oxide. In addition, While studying the rate constant of the dissociation of CO_2 on molten slag (Fe_xO-SiO_2-Al_2O_3-Cu_2O system) by the use of CO_2-CO isotope exchange technique, Coley et al. [36] also concluded that for $[Cu_2O]_o$ < 10 wt. % the concentration of Cu_2O has no effect on the rate constant.

According to the experimental results listed in Table 16, it might be concluded that at 1250°C the reduction rate of ferric oxide increases with the $[Cu_2O]_o$ in the slag and decreases with the increase of Fe/Si mass ratio for additive free system. However, due to some failures in the experiment it was difficult to draw any general conclusion concerning the effect of composition.

Mansoor et al. [80] studied the rate of interfacial reactions between CO_2-CO gas mixtures and CaO-SiO_2-FeO_x slag system (30 wt. % FeO and CaO/SiO_2 = 0.2…2) by the use of CO_2-CO isotope exchange technique. As a result of the study, it was reported that activation energy of the overall reaction, represented in equation (8), vary with the basicity of the slag, as illustrated in Figure 40, but not with the concentration of FeO in the slag.

The dependence of the rate constant of equation (8) on the slag basicity is shown in Figure 41. It can be seen that k increases almost exponentially with basicity. According to the diagram for $CaO/SiO_2 < 1$ at the given temperatures the effect of slag basicity on apparent rate constant seems to be of minor significancy.

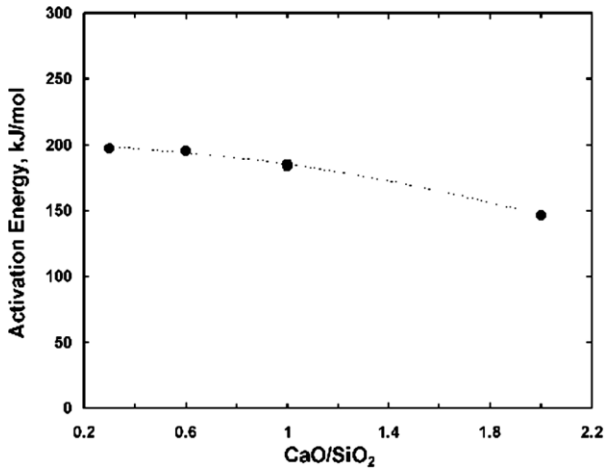

Figure 40. Activation energy of the reaction at unity CO_2/CO as a function of binary basicity of the slag with 30 wt. % FeO [80].

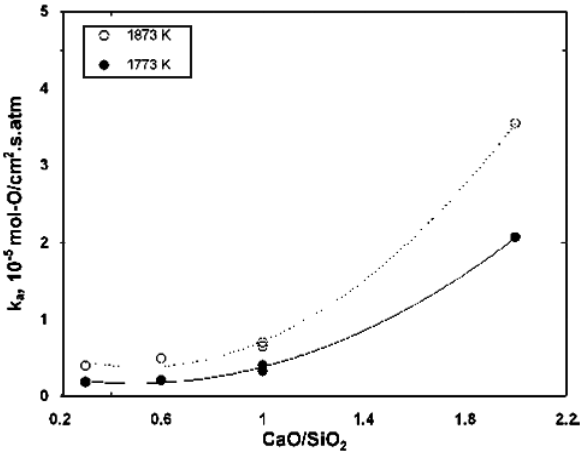

Figure 41. The dependence of the apparent rate constant (at unit CO_2/CO) on the CaO/SiO_2 ratio at 30 wt. % FeO [80].

5 Summary and Conclusions

Advances in the copper smelting technologies to compromise productivity and environmental issues cause to increase copper loss in the oxide form. The extent of copper loss in this form may reach up to 2 wt. % in matte smelting and 20 - 25 wt. % in direct to blister smelting. Thus, copper price - driven slag cleaning in an electric furnace is inevitable. The slag cleaning process involves reduction of Cu_2O by coke, and settling of the produced metal drops and the mechanically entrained metal/matte drops in the slag bath. Mainly convection induced motion of the molten slag and relative velocities of the differently sized drops facilitate collision and then coagulation leading to faster drops settling. The settling rate to the matte layer may also be intensified by optimizing physical properties of the molten slag.

Physical properties of the flash smelting slags vary with variables in the slag cleaning process. Major factors affecting the physical properties are: temperature, partial pressure of oxygen and chemical composition, of which only temperature may be early changed in industrial environments. For optimizing the slag cleaning in the electric furnace the variation range of the physical properties due to the major factors can be summarized as follows: surface tension: 0.33 - 0.43 N/m, density: 2.8 - 3.6 g/cm^3 and dynamic viscosity: 0.05 - 0.3 Pa.s. The values decrease with increasing temperature, except the surface energy. The effect of composition was revealed by different researchers through variation of the amount of the influential slag modifiers like CaO, MgO, SiO_2 and Al_2O_3. For instance, increase in concentration of SiO_2 (in fayalitic type slags (slag V Table 3)) by 20% (from 15 – 35%) causes a decrease in surface energy of the slag by about 15%. Density of the slag decreases linearly with temperature. Viscosity of the slag increases with the increase in Po_2, [Fe_2O_3], [Fe_3O_4] and [SiO_2], while additions of CaO and/or MgO reduce it, with in the viscosity-composition limit.

Temperature in this study was limited to the range 1200 - 1650^{o}C, which is identified to be the most favorable in FSF slags reduction processes. At fixed Fe/SiO_2 ratio and higher oxygen potential addition of CaO(MgO) will reduce Fe^{+3}/Fe^{+2} ratio and copper dissolution (in oxide form) in the slag. This is because the basic oxides will increase the activity coefficient of Fe_2O_3 and replaces some of the Cu^+. Thus, additions of the basic oxides improve the slag cleaning process by reducing the dissolution of copper in the slag and by varying dynamic viscosity, surface tension and density of the slag.

Even though at higher binary basicity than the conventional FSF slags the reduction rate of cuprous oxide given in equation (53) can be assumed to simulate the reduction rate of cuprous oxide by carbon. The reduction rate is autocatalytic resulting in exponential concentration fall once the reduction process starts. The Reduction rate, defined in equation (53), can be numerically expressed as:

$$\frac{\mathrm{d}[\mathrm{Cu_2O}]}{\mathrm{dt}} = -14993.4 \cdot \mathrm{e}^{\frac{-206202}{\mathrm{RT}}} \cdot \frac{[Cu_2O]_t}{[Cu_2O]_o} \cdot \left(1 + 0.95 \cdot \left(1 - \frac{[Cu_2O]_t}{[Cu_2O]_o}\right)\right)$$

Using equation (52) and different slag compositions (Table 18) in the temperature range 1523 - 1673K, the reduction rate of Fe_2O_3, which is found to be the 1st order reaction, can be numerically expressed as:

$$\frac{\mathrm{d}[\mathrm{Fe_2O_3}]}{\mathrm{dt}} = -\psi \cdot 10^{-4} \cdot [\mathrm{Fe_2O_3}]$$

where ψ= 1…8.61, based on the temperature and slag compositions listed in Table 16. According to the above equation, after an hour of the slag-coke reaction, at 1573K, the concentration of Fe_2O_3 in FSF slags will reduce to about 70 % of its initial presence, which may contribute to a decrease in the dynamic viscosity of the slag. Chemical reaction at the slag-coke interface is the most probable rate limiting step in the reduction processes of the two metal oxides. Initial concentration of the cuprous oxide was reported to have no significant influence on the reduction rate. Thus, reduction rate determined for the conventional FSF slag cleaning process may be applied to the Direct - to - Blister slag cleaning process.

Both chemical kinetic and thermodynamic analyses of copper recovery through the carbothermic reaction confirmed that the reduction process improves with temperature rise. At higher temperature, given the supply of carbon is in excess of the amount needed and the slag cleaning process lasts for several minutes, oxidic loss of copper in the FSF slag will eventually be recovered from the reduction point of view. As the Cu_2O reduction by carbon is autocatalytic delayed slag cleaning process may be beneficiary only from the droplets settling point of view.

References

1. Reddy, R. G., Prabhu, V. L. & Mantha, D. Kinetics of reduction of copper oxide from liquid slag using carbon. High-temperature materials and processes. Vol. 22. No1, 2003. pp. 25-33. ISSN 0334-6455.

2. Reddy, R. G., Prabhu, V. L. & Mantha, D. Recovery of copper from copper blast furnace slag. Minerals and Metallurgical Processing. Society for Mining Metallurgy and Exploration. Vol 23, 2006. pp. 97-103.

3. North Carolina Division of Pollution Prevention and Environmental Assistance. Available at: http://www.p2pays.org/.

4. Taskinen, P., Vaarno, J., Jarvi, J., Ahokainen, T. & Laurila, T. Development of a mathematical model of flash smelting and converting process. 3rd international conference on CFD in the minerals and process industries, CSIRO, Melborn, Australia. 2003. pp. 147-154.

5. Davenport, W. G. & Partelpoeg, E. H. Flash Smelting analysis control and optimization. 2nd edition. Pergamon. Oxford. 1987. 324 P.

6. KGHM. Poska Miedz S. A. Available at: http://www.kghm.pl/index.dhtml?category_id=272&lang=en

7. Warczok, A., Riveros, G. & Marin, T., Degel, R., Kunze, J., Oterdoom, H. & Wuebbels, T. Intensive Electrodynamic Slag cleaning. The Carlos Diaz Symposium on pyrometallurgy. Cu2007. Vol. 111(Book 2), 2007. pp. 403-416.

8. Warczok, A. & Riveros, G., Degel, R., Kunze, J. & Oterdoom, H. Slag cleaning in circular and rectangular electric furnaces. Cu2007. Vol. 111(Book 2), 2007. pp. 403-416.

9. Xia, J., Ahokainen, T. & Kankaanpää, T. Parametric study of flow and heat transfer in a slag cleaning furnace. Espoo. Helsinki University of Technology, Laboratory of Materials Processing and Powder Metallurgy. 2003. Espoo. 29 P. ISBN 951-6471-4.

10. White, F. M. Viscous fluid flow. 3rd edition. University of Rhode Island. 2006. 629 P.

11. Gonz´alez, C., Parra, R., Klenovcanova, A., Imris I. & S´anchez, M. Reduction of Chilean copper slags: a case of waste management project. Scandinavian Journal of Metallurgy. 2005. pp. 143–149.

12. Moreno, A., Sánchez, G., Warczok, A. & Riveros, G. Development of slag cleaning process and operation of electric furnace in Las Ventanas Smelter. Empresa Nacional de Minería (ENAMI). Las Ventanas Smelter & Refinery. Chile. (Online accessed 9 Feb 2009).Available at: http://cabierta.uchile.cl/revista/24/articulos/pdf/paper7.pdf

13. Vartiainen, A. Rautasilikaatikuonan viskositeetin ja hiilipelkistys-reaktioiden vaikutus pyrometallurgiseen kuonapuhdistukseen. Lisensiaattityö. TKK, Teknillinen korkeakoulu, Vuoriteolisuusosasto. Espoo. 1983. 211 P.

14. Saarinen, S. Kuonanpuhdistusuunin lämpöhäviöiden lokeellinen lutkimus. Diplömi työ. TKK, Teknillinen Korkeakoulu, Materiali - ja Kalliotekniikan Osasto. Espoo. 2004. 89 p.

15. Ip, S. W. & Toguri, J. M. Entrainment behavior of copper and copper matte in copper smelting operations. Metallurgical and Materials Transactions B. Vol. 23B: No.3. 1992. pp. 303-311.

16. Juusela, M. Modeling of slag and matte discharge from the settler of a copper flash smelting furnace. Licentiate's Thesis. Helsinki University of Technology, Department of Materials Science and Rock Engineering. 2001. 62 p.

17. Carlos, D. Thermodynamic properties of copper-slag systems. INCRA series on the metallurgy of copper. 1974. 178 p.

18. Liukkonen, M. Measuring interfacial energy between liquid iron and slag in equilibrium and reaction conditions. Licentiate's thesis. Helsinki University of Technology, Department of Materials Science and Rock Engineering. Espoo.1998. 102 p.

19. Vargas,S. Straw and Coal Ash Rheology. Ph.D. Thesis. Technical University of Denmark, Combustion and Harmful Emission Control, Department of Chemical Engineering. 2001. 429 p.

20. Vaisburd, S., Brandon, D.G., Kozhakhmetov, S. & Kenzhaliyev, E. Physicochemical properties of matte-slag melts taken from Vanyukov's furnace for copper extraction. Metallurgical and materials transactions B. Vol. 33B. 2002. pp. 561-564.

21. Nowok, J.W., Hurley, J.P. & Bleber, J.A. The cause of surface tension increase with temperature in multicomponent aluminosilicates derived from coal-ash slags. Juornal of materials Science. Energy and environmental research center, fuels and materials science. 1995. pp. 361-164.

22. Utigard,T. Surface and interfacial tensions of iron based systems. ISIJ International. Vol. 34. 1994. pp. 951-959.

23. Goñi, C. & Sanchez, M. Modeling of copper content variation during "El Teniente" slag cleaning process. Nonferrous pyrometallurgy. Molten 2009. Santiago, Chile. 2009. pp.1203-1210.

24. Timothy, V. J. The kinetics of reduction of iron from silicate melts by carbon- monoxide – carbon dioxide gas mixtures at 1300^{o}C. PhD thesis. Massachusetts Institute of Technology, Department of Materials Science and Engineering. 1987. 207 p.

25. Hiroyuki, F., Jeffrey, R. D. & James, M. T. Wetting Behavior between Fayalite-Type Slags and Solid Magnesia. Department of Metallurgy and Materials Science. University of Toronto. J. Am.Ceram. Soc. 80. 1997. pp. 2229-2236.

26. Haiping, S. Reaction Rates and Swelling Phenomenon of Fe–C Droplets in FeO Bearing Slags. ISIJ International. Vol. 46: No. 11. 2006. pp.1560–1569.

27. Siddiqi, N., Bhoi, B., Paramguru, R. K., Sahajwalla. V. & Ostrovski, O. Slag–graphite wettability and reaction kinetics Part 2. Wettability influenced by reduction kinetics. Ironmaking & steelmaking. 2000. vol. 27: No 6. p. 437-441. ISSN 0301-9233.

28. Bhoi, B., Ray, H.S. & Sahajwalla, V. Influence of different parameters on wettability of graphite by CaO-SiO_2-FeO molten slag. IE(I) Journal-MM. Vol 89. 2008. pp. 3-8.

29. Elliot, B.J., See, J.B. & Rankin, W.J. Trans. Inst. Min. Metal. 1978. Vol. 87. p. C204-211.

30 Nakamura, T., Noguchi, F., Ueda, Y. & Nakajyo, S. J. Min. Metall. Inst. Japan. 1988. Vol. 104. pp. 531-36.

31. Donald, B., Dingwell & Mark, B. Melt densities in the CaO-FeO-Fe_2O_3-SiO_2 system and the compositional dependence of the partial molar volume of ferric iron in silicate melts. Geochimica et Cosmochimica. Vol. 52. 1988. pp. 2815-2825.

32. Wikipedia. The free encyclopedia. Available at: http://en.wikipedia.org/wiki/MainPage .

33. Jimbo, I. & Cramb, A. W. The density of liquid iron-carbon alloys. Metallurgical Transactions B, Vol. 24B. 1993. pp. 5-15.

34. Loos, T. & Lossin, A. Investigation of the silica slag of Norddeutsche Affinere's Flash Furnace. The Carlos Diaz Symposium on pyrometallurgy. Cu2007. vol. 111(Book 2). 2007. pp. 417-427.

35. Fruehan, R.J. Clean steel technology. POHTO – The institute for management and technological training. 2005.

36. Chen, E. & Coley, K. Gas slag reaction in cleaning of copper slags. Canadian Metallurgical Quaterly. Vol. 45: No.2, 2006. pp. 167- 174.

37. Zhao, B., Font, J., Moyano, A., Jak, E. & Hayes, P. C. Viscosity and electrical conductivity of copper slag at controlled oxygen potential. Molten 2009. VIII International conference on molten slags. Fluxes and salts . 2009. 14 p.

38. Dusan, B., Fernando, P., Roberto, P., Erwin, U., Jose, P., Mitsutaka, H., Felipe, C., Armando S. & Mario, S. Recovery of Iron from Copper Flash Smelting Slags. Molten 2009. Santiago. Chile. 2009. pp.621-628.

39. Jalkanen, H. Studies on matte-slag equilibria in the system Cu-Fe-S-O-SiO_2. Report TKK-V-A1. Helsinki. Helsinki University of Technology, Institute of Process Metallurgy. 1977. 92 p. ISBN 951-751-130-2.

40. Henao, H., Hayes, P., Jak, E., George-Kennedy, D. & Nexhip, C. Investigation of copper smelting slags in the FeO-Fe_2O_3-SiO_2-CaO-MgO-Al_2O_3 system at fixed oxygen potential. Molten 2009. Santiago. Chile. 2009. pp. 93-100.

41. Henao, H., Hayes, P., Jak, E., H., Pizarro, C., Font, J. & Moyano, A. Phase Equilibrium of Fayalite-Based Slags for the Slag Cleaning Process in Copper Production. Molten 2009. Santiago. Chile.2009. pp. 83-91.

42. Zhao, B., Jak, E. & Hayes, P.C. The effect of Al_2O_3 on liquidus temperatures of faylite slags. Metallurgical and materials transactions B. Vol. 30B. 1999. pp. 597-605.

43. Kim, H. G. & Sohn, H. Y. Effects of CaO, Al_2O_3 and MgO additives on the copper solubility, Ferric/Ferrous ratio, and minor element behavior of iron-silicate slags. Materials and Metallurgical Transactions B. Vol. 29B. 1998. pp. 411-418.

44. Yazawa, A., Takeda, Y. & Nakazawa, S. Ferrous calcium silicate slag to use for copper smelting and converting. Copper99 –cobre99 Final technical program. 1999. 58 p.

45. Antrekowitsch, H., Wenzl, C., Filzwieser, I. & Offenthaler, D. Pyrometallurgical Refining of Copper in an Anode Furnace. TMS (The Minerals, Metals & Materials Society).

46. Terry, B.S., harris, C.L. Kinetics of reduction of metal values from fayalite-based slags – part 1: reduction of nickel and copper. The Instution of Mining and Metallurgy. 1995. pp. 81-91.

47 Nagamori, M., Mackey, P.J. & Torassoff, P. Metallurgical Transactions B. 1995. Vol. 6B. pp. 295- 301.

48. Degterov, S. A. & Pelton, A. D. A Thermodynamic database for copper smelting and converting. Metallurgical and Materials Transactions B. Process Metallurgy and Materials Processing Science. Vol. 30B: n°4.1999. pp. 661-669.

49. Roine, A. HSC Chemistry 5.11. Outokumpu Research Oy.

50. Terry, B.S., harris, C.L. Kinetics of reduction of metal values from fayalite-based slags – part 2: modeling of idealized slag-cleaning conditions. The Instution of Mining and Metallurgy. 1995. pp. 92-101.

51. Seppänen, R., Kevinen, M. & Haavisto, A. Matemaattisten Aineiden Opettajien Liitto (MAOL)-Taulukot matematiikka, fysiikka ja kemia.1991. 157 p. ISBN 951-1-12112-X.

52. Hayes, P.C., Okongwu, D.A. & Toguri, J.M. Some observations of the reactions between molten oxides and solid carbon. Canadian metallurgical quarterly. Vol. 34. No. 1. 1995. pp 27- 36.

53. Tae, W.K., Sushil, G., Saha-Chaudhury, N. & Veena, S. Wetting and Interfacial Reaction Investigations of Coke/Slag systems and Associated Liquid Permeability of Blast Furnances. ISIJ International. Vol.45: No.11. 2005. pp. 1526-1535.

54. Gleixner, S. Heterogeneous nucleation. Solid state kinetics. San Jose State University. Available at: http://www.engr.sjsu.edu/sgleixner/mate152/Lecture%20Notes/W11_hetero_nucleation.pdf

55. Mazur, A. & Gasik, M. In-situ analysis of phase formations in semi-solid state in the hypereutectic Al-Si alloy. Helsinki University of Technology-TKK. 2008. pp. 63-69.

56. Nucleation in metals and alloy. Matter. University of Liverpool. Available at: http://www.matter.org.uk/matscicdrom/manual/nu.html

57. Tarek El Gammal, I. The significance of interfacial phenomena in the metallurgical processes. Institute of Ferrous Metallurgy. Aachen University of Technology. Available at: http://www.ariel.ac.il/management/research/pf/zinigrad/mmt/MMT-2000/papers/547-557.doc.

58. Haiping, S. & Wesley, E. Interfacial phenomenon and reaction kinetics between the carbon and slag in iron making process. Energy and fuels. 2007. 21(2). pp. 413-418. Available at: http://pubs.acs.org/doi/pdf/10.1021/ef060402d?cookieSet=1

59. Fuchikami, N., Ishioka, S. & Kiyono, K. Simulation of a Dripping Faucet. Department of physics, Tokyo Metropolitant University.1998. 24 p.

60. Zhijun, H. Bubble bursting phenomena on the free surface of iron melt and at the slag/iron interface. Acta Polytechnica Scandinavica. Chemical Technology and Metallurgy series No. 286.Espoo. Helsinki University of Technology, Laboratory of Metallurgy. 2001. 98 p. ISBN 951-666-584-5.

61. Blomster, K. Heterogeeninen kinetiikka. TKK. 1971. 53 s.

62. Asteljoki, J. Eräitä näkökohtia heterogeenisten reaktioiden kinetiikasta. TKK. 1972. 50 s.

63. Härkki, J. & Angerman, M. Pinnan rakenteen merkitys kiinteä-kaasu reaktiossa. POHTO-sarja B, 65 (1997), s. 4/1-25.

64. Gasik, M. Pelkistysprosessien kinetiikka ja kokeelliset menetelmät. POHTO-sarja B, 79 (2001), s. 1/1-41.

65. Brown, M. E., Dollimore, D. & Galway, A. K. Reactions in solid state, In:" Comprehensive Chemical Kinetics". Vol. 22. eds. C. H. Bamford, C. F. Tipper, Amsterdam.1980. 340 p.

66. Flammersheim, H.J., Eckardt, N., & Opfermann J. Thermochim. Acta, 229 (1993). 281 p.

67. Laitinen, R. & Toivonen, J. Yleinen ja epäorgaaninen kemia. Kemian perusteet 1-2. Otakustantamo, 477, Espoo, 1984, 312 s.

68. Malek, J., Sausestak, J., Rouquerol, F., Rouquerol, J., Criado, J., Ortega, A. & In: J. Thermal Analysis, 38. 1992. 71 p.

69. Opfermann, J., Wilke, G., Ludwig, W., Hagen, S., Gebhardt, M. & Kaisersberger E. ”Thermische Analyseverfahren in Industrie und Forschung”, VI. Herbstschule Meisdorf, Friedrich-Schiller-Universität.1991.

70. Brown, M. E. “Introduction to Thermal Analysis, Techniques and Applications”. Chapman and Hall Publ., London, New York. 1989.

71. Flammersheim, H. J. & Opfermann, J. Thremochimica Acta, 337 (1999), pp. 141-153.

72. Gasik, M. Metallurgisten prosessien kinetiikka, Reaktioiden kinetiikka ja mekanismit. POHTO. Oulu. 2005. 17 p.

73. Sohn, H.Y. & Korean J. Chem. Eng., 20(2). 2003. pp. 185-199.

74. Durbin, J. & Watson, G.S. Biometrika, 58 (1971) 1.

75. Morales, R.D., Rodriguez-Hernández, H., Garnica-Gonzälez, P. & Romero-Serrano, J.A. A mathematical model for the reduction kinetics of iron oxide in electric furnace slags by graphite injection. ISIJ International. Vol. 37. No. 11. 1997. pp. 1072-1080.

76. Xie, H., Schulz, M. & Oeters, F. Kinetics of iron oxide reduction from CaO-MgO-FeOn-SiO_2 slags by silicon dissolved in liquid iron. Process metallurgy, Steel research 67. No.8. 1996. pp. 307-313.

77. Warczok, A., Riveros, G., Degel, R., Kunze, J. and Oterdoom,, H. Computer simulator of slag cleaning in an electric furnace. The Carlos Diaz symposium on pyrometallurgy. Cu2007. vol. 111(Book 2). 2007. pp. 367-378.

78. Min, D.J., Han, J.W. and Chung, W.S. A Study of the reduction rate of FeO in slag by solid carbon. Metallurgical and Materials Transactions B. vol. 30B. 1999. pp. 215-221.

79. El-Rassi, K.P. and Utigard, T.A. Rate of slag reduction in laboratory electric furnace-alternating vs direct. Metallurgical and materials transactions B. Vol. 31B. 2000.

80. Mansoor, B. & Kenneth, S. C. Kinetics of CO-CO_2 reaction with CaO-SiO_2-FeO_x melts. McMaster University. Department of Materials Science and Engineering. 2004. pp.169-178.

81. Sjöden, O., Seetharaman, S. & Staffansson, L. I. On the Gibbs energy of formation of wustite. Metallurgical Transactions B. Vol. 17B. 1986. pp. 179 - 186.

Appendix A

Outokumpu's flash smelting process with its adjacent equipments. Fossil fuel handling facilities are not shown [5].

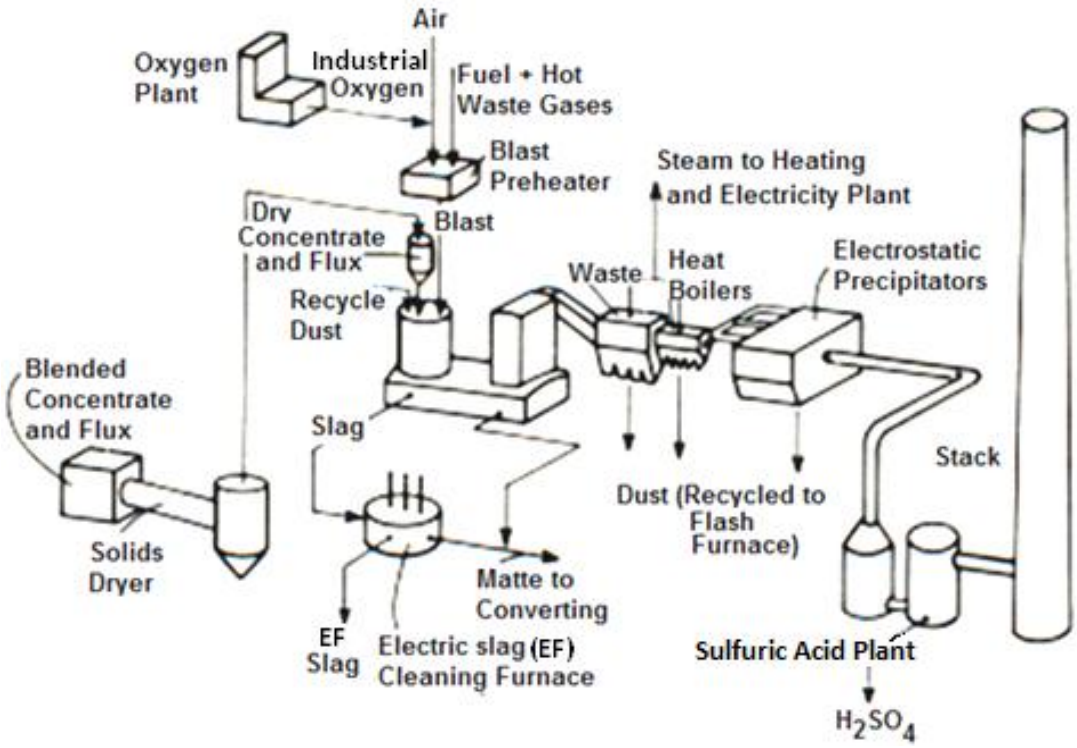

Appendix B

Schematic 3D diagram of the electric furnace under operation with the dominant reactions in the copper flash smelting slag cleaning process.

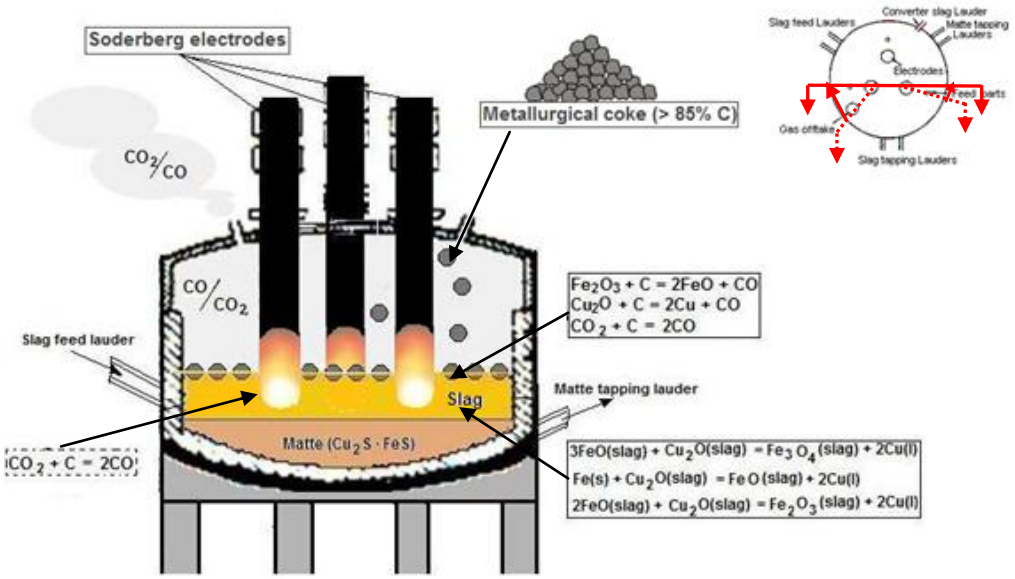

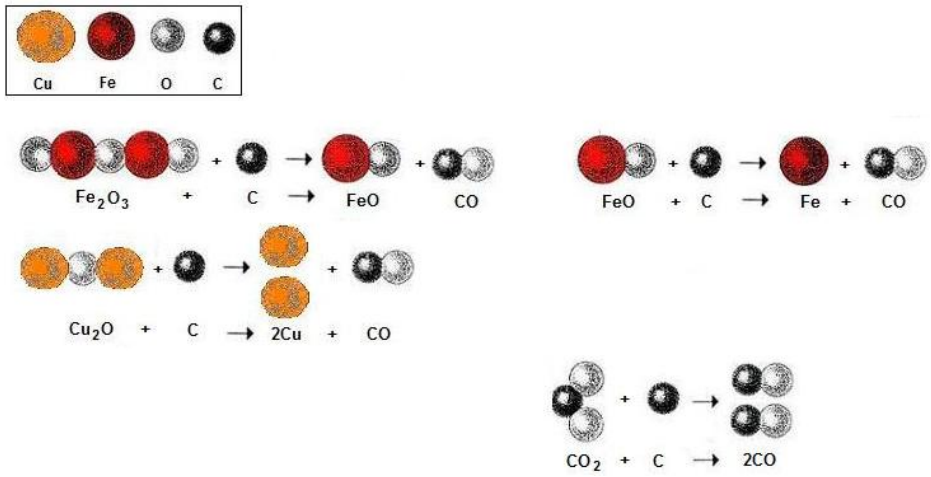

Appendix C

The Ellingham diagram showing the standard free energy of formation of oxides versus temperature. Equilibrium partial pressure of oxygen and the CO/CO_2 ratio corresponding to the temperature and the standard free energy are shown adjacently [81].

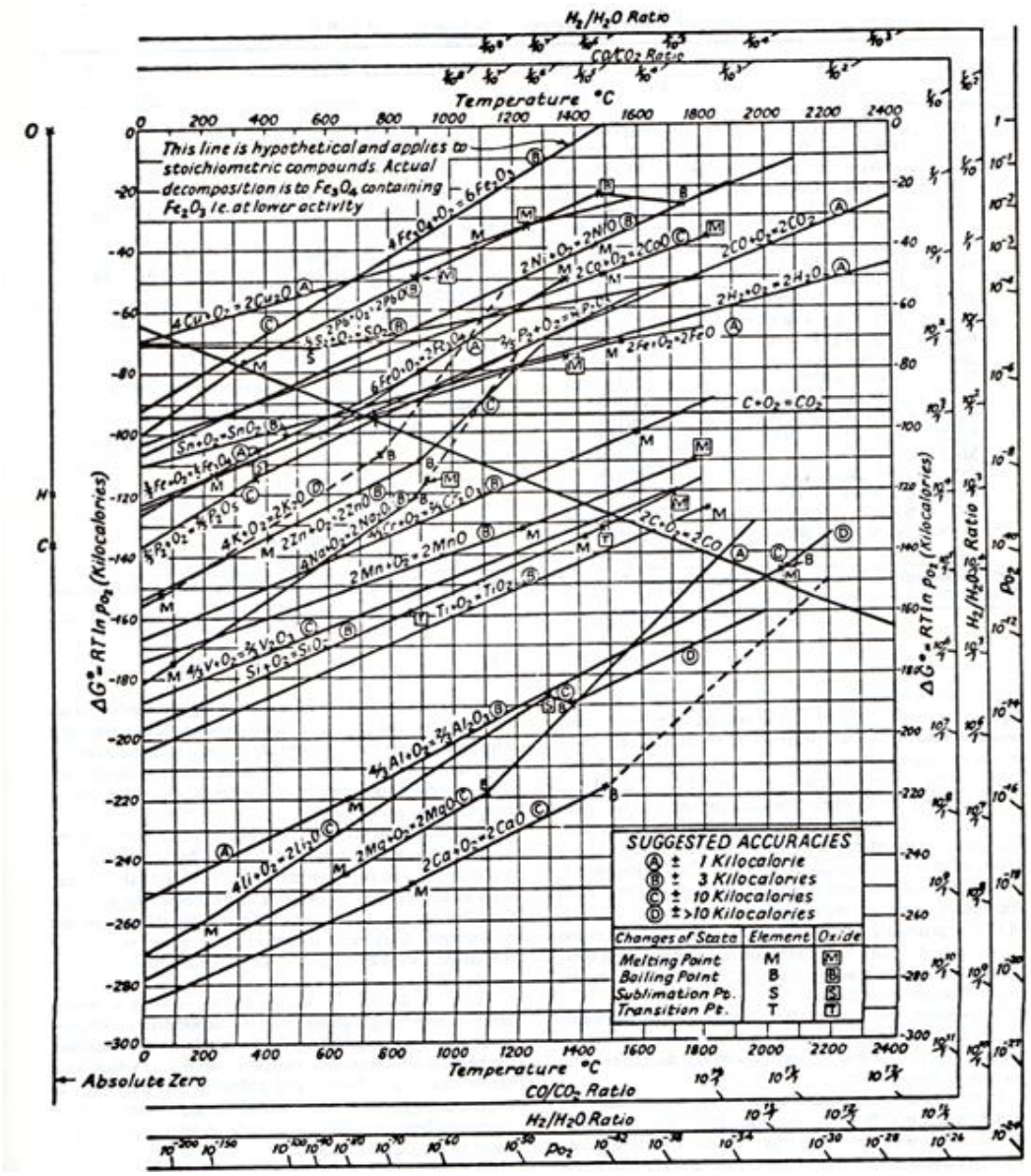

Appendix D

Standard Gibbs free energy of reduction reactions at 1573K [2, 11, 49].

Reaction	$\Delta H(KJ)$	$\Delta S(J/K)$	$\Delta G(kJ/mol)$
$(FeO)_{slag} + C = [Fe]_{metal} + CO(g)$	137.42	143.25	-87.92
$(Cu_2O)_{slag} + C = 2[Cu]_{metal} + CO(g)$	8.6	130.44	-196.59
$CO_2(g)+C=2CO(g)$	164.36	170.39	-103.67
$(CuO_{0.5})_{slag} + (FeO)_{slag}= Cu +Fe_2O_3$	-	-	-15.1
$Fe_3O_4(s)+3/2SiO_2(s)=3/2(2FeO.SiO_2(l))+CO_2(g)$	41.11	63.35	-58.54
$½(2FeO·SiO_2(l))+CO(g)=Fe(l)+ ½SiO_2(s)+CO_2(g)$	-20.89	-32.34	30
$½SiO_2(s)+CO(g)= ½Si(l)+CO_2(g)$	194.02	15.07	170.32
$½SiO_2(s)+CO(g)= ½Si(s)+CO_2(g)$	168695	0.36	168.13

Appendix E

A calculation framework in an excel-work sheet for calculating the Gibbs free energy change of the dominant reactions in the slag reduction process. Picture taken at a particular temperature and activities of the slag components.

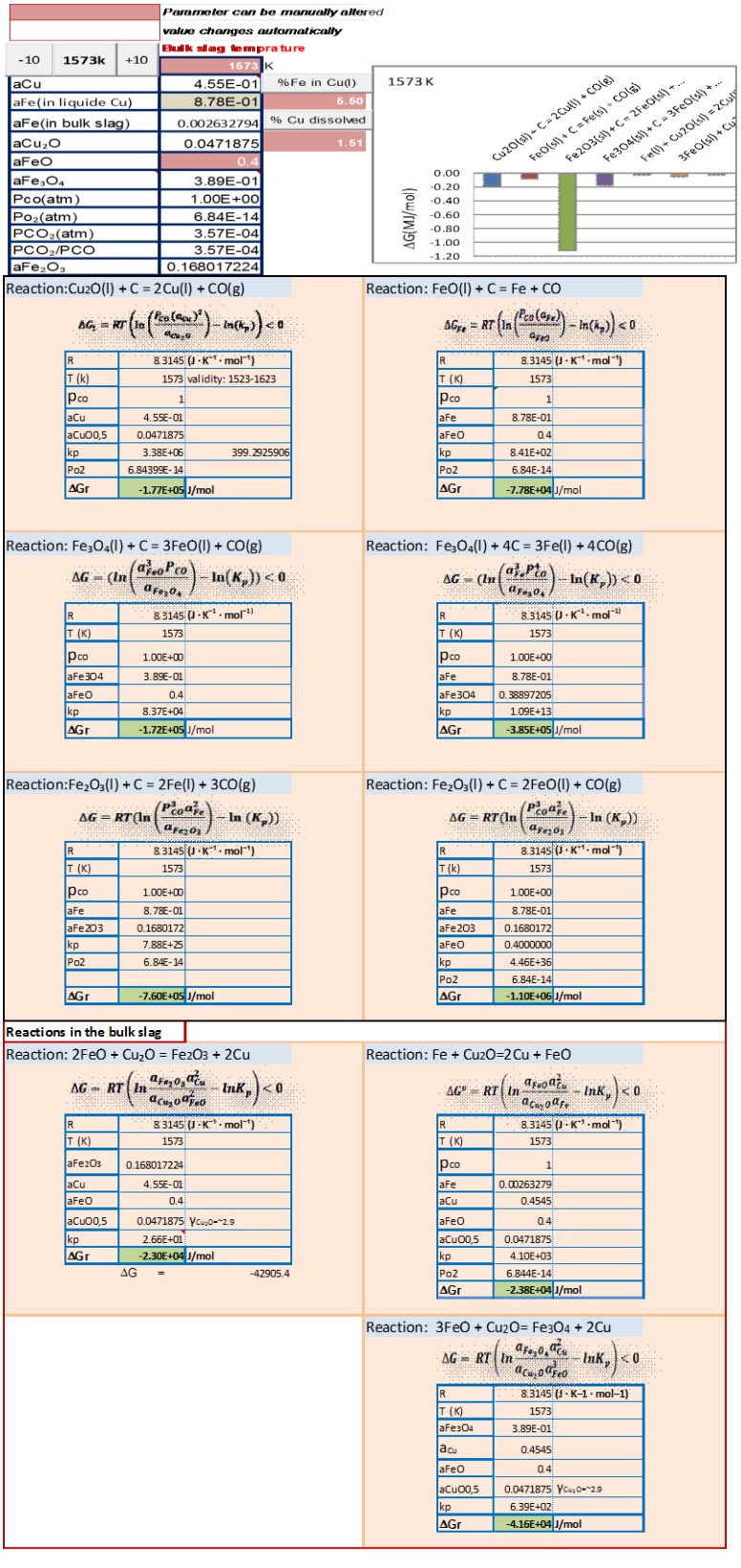

Parameter can be manually altered
value changes automatically
Bulk slag tempra ture

-10	1573k	+10	1573 K
aCu	4.55E-01	%Fe in Cu(l)	
aFe(in liquide Cu)	8.78E-01	5.60	
aFe(in bulk slag)	0.002632794	% Cu dissolved	
aCu_2O	0.0471875	1.51	
aFeO	0.4		
aFe_3O_4	3.89E-01		
Pco(atm)	1.00E+00		
Po_2(atm)	6.84E-14		
PCO_2(atm)	3.57E-04		
PCO_2/PCO	3.57E-04		
aFe_2O_3	0.168017224		

Reaction: $Cu_2O(l) + C = 2Cu(l) + CO(g)$

$$\Delta G_1 = RT\left(\ln\left(\frac{P_{CO}(a_{Cu})^2}{a_{Cu_2O}}\right) - \ln(k_p)\right) < 0$$

R	8.3145	$(J \cdot K^{-1} \cdot mol^{-1})$
T (k)	1573	validity: 1523-1623
Pco	1	
aCu	4.55E-01	
aCuO0,5	0.0471875	
kp	3.38E+06	399.2925906
Po2	6.84399E-14	
ΔGr	-1.77E+05	J/mol

Reaction: $FeO(l) + C = Fe + CO$

$$\Delta G_{Fe} = RT\left(\ln\left(\frac{P_{CO}(a_{Fe})}{a_{FeO}}\right) - \ln(k_p)\right) < 0$$

R	8.3145	$(J \cdot K^{-1} \cdot mol^{-1})$
T (K)	1573	
Pco	1	
aFe	8.78E-01	
aFeO	0.4	
kp	8.41E+02	
Po2	6.84E-14	
ΔGr	-7.78E+04	J/mol

Reaction: $Fe_3O_4(l) + C = 3FeO(l) + CO(g)$

$$\Delta G = (ln\left(\frac{a_{FeO}^3 P_{CO}}{a_{Fe_3O_4}}\right) - \ln(K_p)) < 0$$

R	8.3145	$(J \cdot K^{-1} \cdot mol^{-1})$
T (K)	1573	
Pco	1.00E+00	
aFe3O4	3.89E-01	
aFeO	0.4	
kp	8.37E+04	
ΔGr	-1.72E+05	J/mol

Reaction: $Fe_3O_4(l) + 4C = 3Fe(l) + 4CO(g)$

$$\Delta G = (ln\left(\frac{a_{Fe}^3 P_{CO}^4}{a_{Fe_3O_4}}\right) - \ln(K_p)) < 0$$

R	8.3145	$(J \cdot K^{-1} \cdot mol^{-1})$
T (K)	1573	
Pco	1.00E+00	
aFe	8.78E-01	
aFe3O4	0.38897205	
kp	1.09E+13	
ΔGr	-3.85E+05	J/mol

Reaction: $Fe_2O_3(l) + C = 2Fe(l) + 3CO(g)$

$$\Delta G = RT(\ln\left(\frac{P_{CO}^3 a_{Fe}^2}{a_{Fe_2O_3}}\right) - \ln(K_p))$$

R	8.3145	$(J \cdot K^{-1} \cdot mol^{-1})$
T (K)	1573	
Pco	1.00E+00	
aFe	8.78E-01	
aFe2O3	0.1680172	
kp	7.88E+25	
Po2	6.84E-14	
ΔGr	-7.60E+05	J/mol

Reaction: $Fe_2O_3(l) + C = 2FeO(l) + CO(g)$

$$\Delta G = RT(\ln\left(\frac{P_{CO}^3 a_{Fe}^2}{a_{Fe_2O_3}}\right) - \ln(K_p))$$

R	8.3145	$(J \cdot K^{-1} \cdot mol^{-1})$
T (k)	1573	
Pco	1.00E+00	
aFe	8.78E-01	
aFe2O3	0.1680172	
aFeO	0.4000000	
kp	4.46E+36	
Po2	6.84E-14	
ΔGr	-1.10E+06	J/mol

Reactions in the bulk slag

Reaction: $2FeO + Cu_2O = Fe_2O_3 + 2Cu$

$$\Delta G = RT\left(ln\frac{a_{Fe_2O_3}a_{Cu}^2}{a_{Cu_2O}a_{FeO}^2} - lnK_p\right) < 0$$

R	8.3145	$(J \cdot K^{-1} \cdot mol^{-1})$
T (K)	1573	
aFe2O3	0.168017224	
aCu	4.55E-01	
aFeO	0.4	
aCuO0,5	0.0471875	γ_{Cu_2O}=2.9
kp	2.66E+01	
ΔGr	-2.30E+04	J/mol
ΔG =	-42905.4	

Reaction: $Fe + Cu_2O = 2Cu + FeO$

$$\Delta G^o = RT\left(ln\frac{a_{FeO}a_{Cu}^2}{a_{Cu_2O}a_{Fe}} - lnK_p\right) < 0$$

R	8.3145	$(J \cdot K^{-1} \cdot mol^{-1})$
T (K)	1573	
Pco	1	
aFe	0.00263279	
aCu	0.4545	
aFeO	0.4	
aCuO0,5	0.0471875	
kp	4.10E+03	
Po2	6.84E-14	
ΔGr	-2.38E+04	J/mol

Reaction: $3FeO + Cu_2O = Fe_3O_4 + 2Cu$

$$\Delta G = RT\left(ln\frac{a_{Fe_3O_4}a_{Cu}^2}{a_{Cu_2O}a_{FeO}^3} - lnK_p\right) < 0$$

R	8.3145	$(J \cdot K-1 \cdot mol-1)$
T (K)	1573	
aFe3O4	3.89E-01	
aCu	0.4545	
aFeO	0.4	
aCuO0,5	0.0471875	γ_{Cu_2O}=2.9
kp	6.39E+02	
ΔGr	-4.16E+04	J/mol

Appendix F

Gibbs free energy change of the reduction reactions as a function of temperature and activity of the slag components.

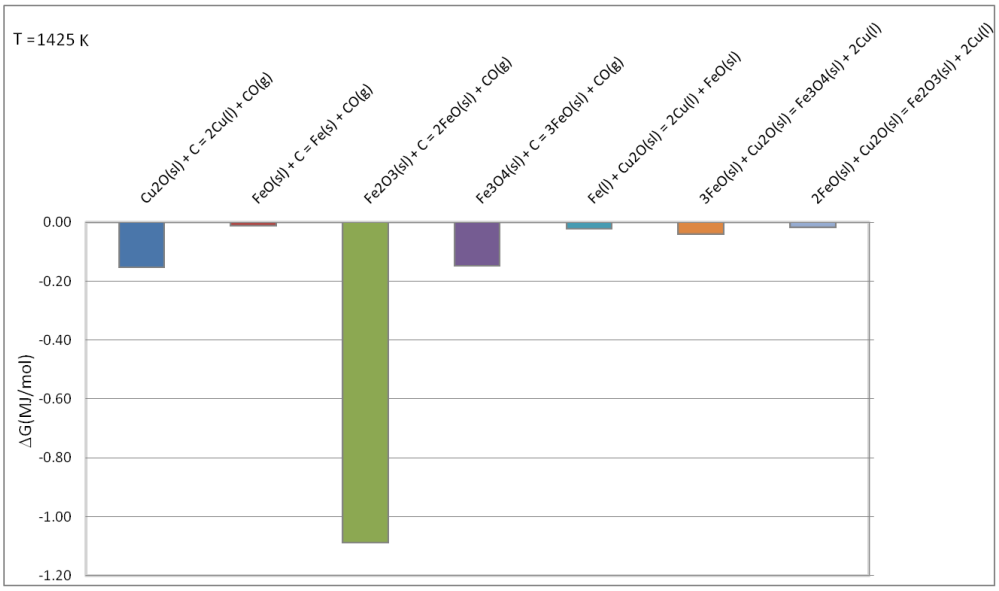

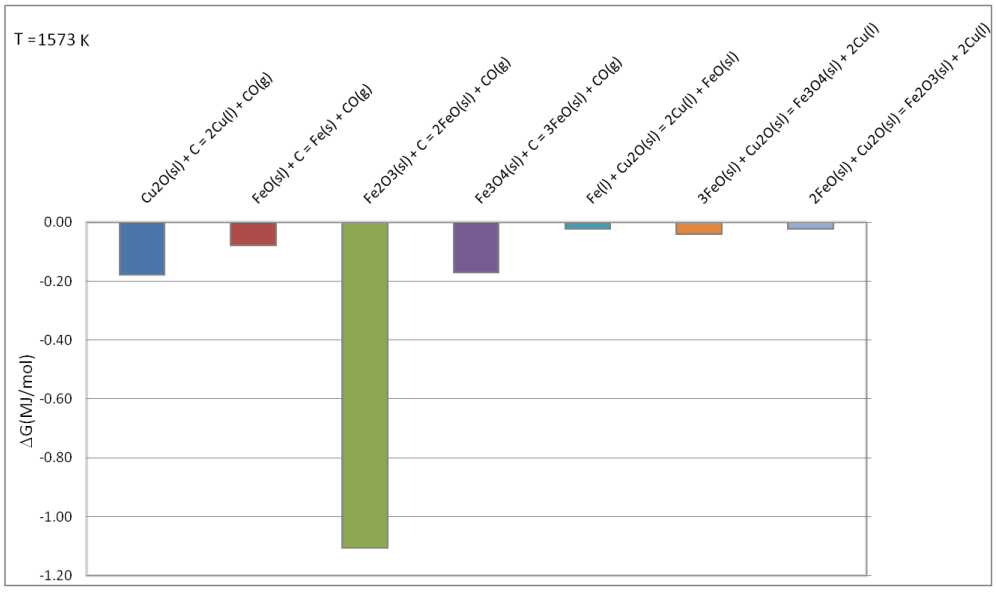

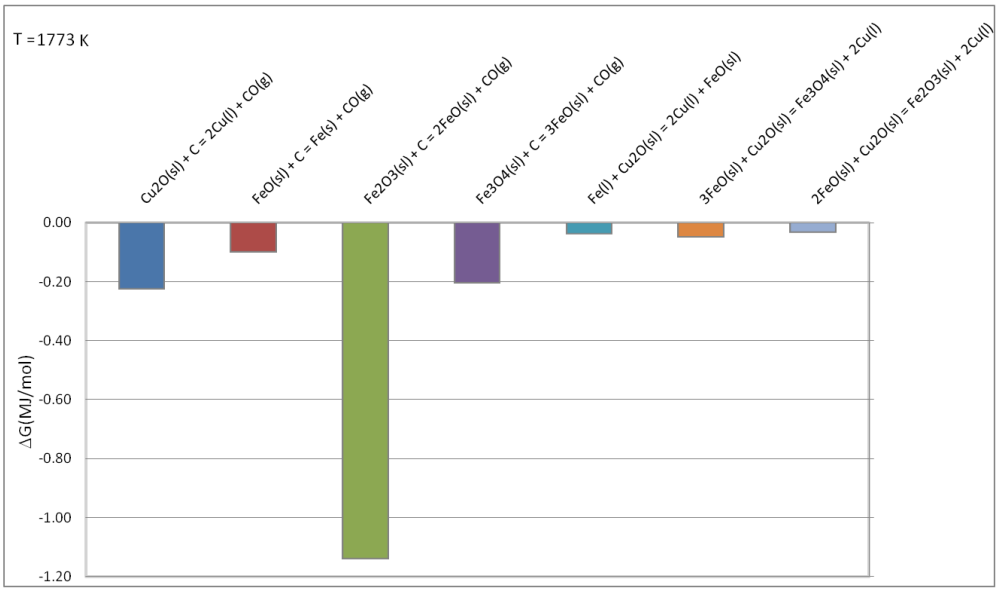
T =1773 K
Cu2O(sl) + C = 2Cu(l) + CO(g)
FeO(sl) + C = Fe(s) + CO(g)
Fe2O3(sl) + C = 2FeO(sl) + CO(g)
Fe3O4(sl) + C = 3FeO(sl) + CO(g)
Fe(l) + Cu2O(sl) = 2Cu(l) + FeO(sl)
3FeO(sl) + Cu2O(sl) = Fe3O4(sl) + 2Cu(l)
2FeO(sl) + Cu2O(sl) = Fe2O3(sl) + 2Cu(l)
0.00
-0.20
-0.40
-0.60
-0.80
-1.00
-1.20
ΔG(MJ/mol)